Aerosol optical properties and radiative forcing based on synchronous measurements of China Aerosol Remote Sensing Network (CARSNET) over eastern China

Huizheng Che[1*], Bing Qi[2], Hujia Zhao[1], Xiangao Xia[3,4], Philippe Goloub[5], Oleg Dubovik [5], Victor Estelles[6] , Emilio Cuevas-Agulló[7], Luc Blarel[3], Yunfei Wu[8], Jun Zhu[9], Rongguang Du[2], Yaqiang WANG[1], Hong Wang[1], Ke Gui[1], Jie Yu[1], Yu Zheng[9], Tianze Sun[1], Quanliang Chen[10], Guangyu Shi[11], Xiaoye Zhang[1*]

1 State Key Laboratory of Severe Weather (LASW) and Institute of Atmospheric Composition, Chinese Academy of Meteorological Sciences, CMA, Beijing, 100081, China

2 Hangzhou Meteorological Bureau, Hangzhou, 310051, China

3 Laboratory for Middle Atmosphere and Global Environment Observation (LAGEO), Institute of Atmospheric Physics, Chinese Academy of Sciences, Beijing, 100029, China

4 School of Geoscience University of Chinese Academy of Science, Beijing, 100049, China

5 Laboratoire d'Optique Amosphérique, Université des Sciences et Technologies de Lille, 59655, Villeneuve d'Ascq, France

6 Dept. Fisica de la Terra i Termodinamica, Universitat de Valencia, C/ Dr. Moliner 50, 46100 Burjassot, Spain

7 Centro de Investigación Atmosférica de Izaña, AEMET, 38001 Santa Cruz de Tenerife , Spain

8 Key Laboratory of Regional Climate-Environment for Temperate East Asia, Institute of Atmospheric Physics, Chinese Academy of Sciences, Beijing 100029, China

9 Collaborative Innovation Center on Forecast and Evaluation of Meteorological Disasters, Nanjing University of Information Science & Technology, Nanjing 210044, China

10 Plateau Atmospheric and Environment Key Laboratory of Sichuan Province, College of Atmospheric Sciences, Chengdu University of Information Technology, Chengdu, 610225, China

11 State Key Laboratory of Numerical Modeling for Atmospheric Sciences and Geophysical Fluid Dynamics (LASG), Institute of Atmospheric Physics, Chinese Academy of Sciences, Beijing, 100029, China

Corresponding author: chehz@camscma.cn & xiaoye@camscma.cn

Abstract

Variations in the optical properties of aerosols and their radiative forcing were investigated based on long-term synchronous observations made at three-minute intervals from 2011 to 2015 over seven adjacent CARSNET (China Aerosol Remote Sensing NETwork) urban (Hangzhou), suburban (Xiaoshan, Fuyang, LinAn, Tonglu, Jiande) and rural (ChunAn) stations in the Yangtze River Delta region, eastern China. The fine-mode radii in the Yangtze River Delta region were ~0.2–0.3 μm with a volume fraction of 0.10–0.12 μm^3 and the coarse-mode radii were ~2.0 μm with a volume fraction close to 0.07 μm^3. The fine-mode aerosols were obviously larger in June and September than in other months at almost the sites. The aerosol optical depth (AOD at 440nm) varied from 0.68 to 0.76, with two peaks in June and September, and decreased from the eastern coast to western inland areas. The fine mode fraction to the total AOD was >0.90 and the extinction Angström exponent was >1.20 throughout the year at all seven sites. The AOD at 500nm has also been studied because of the wavelength dependent of optical properties to show the monthly and diurnal cycle. The MODIS/Terra C6 retrieval AOD values was generally more stable in the YRD region compared with the MODIS/Aqua product with the two Deep Blue (10km) and Dark Target (3km and 10km) methods against ground-based observations. The single-scattering albedo varied from 0.91 to 0.94, indicating that scattering aerosol particles are dominant in this region. Large imaginary parts of the refractive index were seen in August at all urban, suburban and rural sites. The absorption AOD was low in the winter. The absorption Angström exponent and the extinction Angström exponent shows that the “mostly dust” category was very low in the suburban and rural sites (<0.01%) and also less in the urban site (~0.24%). The aerosols caused negative radiative forcing both at the Earth’s surface and at the top of the atmosphere all year round in the Yangtze River Delta region with the lower surface albedo in a unique geographical climate condition of better vegetation in the YRD region than in north/northeast China.

1. Introduction

Aerosols have important effects on the Earth’s climate at both global and regional scales, although there are still great uncertainties in assessing their impact (Hansen et al.2000; Solomon et al., 2007; Schwartz and Andreae, 1996). Aerosols affect not only the radiative balance of the Earth–atmosphere system by directly scattering and absorbing solar radiation (Charlson et al., 1992; Ackerman and Toon, 1981), but also indirectly affect the climate through aerosol‑cloud interactions (Twomey et al., 1984; Albrecht et al., 1989; Li et al., 2016).

The optical properties of aerosols influence the aerosol radiative balance and can be used to predict and assess global and regional changes in the Earth's climate (Eck et al., 2005; Myhre et al., 2009; IPCC, 2013; Panicker et al., 2013). Long-term, ground-based observations are crucial to our understanding of the global and regional variations in the optical properties of aerosols and their effects on the Earth's climate (Holben et al., 2001; Kaufman et al., 2002; Sanap and Pandithurai, 2014; Li et al., 2016). Ground-based monitoring networks have been established worldwide—for instance, AERONET (Aerosol Robotic Network) (Holben et al.,1998; Goloub et al., 2007), SKYNET (SKYrad Network) (Takamura et al., 2004), EARLINET (European aerosol Lidar network) (Pappalardo et al.,2014) and the GAW-PFR Network (Global Atmosphere Watch Programmer-Precision Filter Radiometers) (Wehrli, 2002; Estelles et al., 2012).The above networks exclude EARLINET include several automated sites in China. CARSNET (the China Aerosol Remote Sensing NETwork) (Che et al., 2009a, 2015b) and CSHNET (the Chinese Sun Hazemeter Network) were established to obtain data on aerosol optical characteristics in China (Xin et al., 2007).

Most of the ground-based studies of the optical properties of aerosols in China have been concentrated in urban regions undergoing rapid economic development, which have high aerosol loadings and serious environmental problems (Cheng et al., 2015; Pan et al., 2010; Xia et al., 2013; Wang et al., 2015; Che et al., 2015a). Analyses of the aerosol optical depth (AOD), the types of aerosols and the classification of ambient aerosol populations based on their size and absorption properties(Giles et al., 2011) are needed to understand their effects on the Earth's climate and environment (Che et al., 2009b; Wang et al., 2010; Zhu et al., 2014).

The Yangtze River Delta (YRD) region in eastern China has undergone rapid economic growth and has high emissions of aerosols (Fu et al., 2008; Zhang et al., 2009).There have been many studies of the optical properties of aerosols in eastern China and these are important in our understanding of both the local air quality and regional climate change (Duan and Mao, 2007; Pan et al., 2010; Ding et al., 2016). Basic investigations of the variation in the optical characteristics of aerosols over the YRD region have been carried out at Nanjing, Hefei, Shanghai, Shouxian and Taihu (Zhuang et al. 2014; Li et al., 2015; Wang et al., 2015; He et al., 2012; Lee et al., 2010; Cheng et al., 2015; Xia et al., 2007). These studies in the YRD region have mostly been single-site and/or short-period investigations. The study sites are ~100 km apart from each other, which makes high spatial resolution satellite and modeling validations difficult. Thus there is still a lack of long-term, continuous and synchronous observations of the optical characteristics of aerosols, especially over adjacent urban, suburban and rural areas in the YRD region.

High-frequency ground-based observations of the variations in the optical characteristics of aerosols are necessary to our understanding of the processes involved in air pollution (e.g. the source, transport and diurnal variations of the pollution) and their effect on the regional climate. Ground-based observations are also important in the validation and improvement of satellite retrieval data (Holben et al., 2017; Xie et al., 2011). A high density of ground-based sun-and sky-scanning spectral radiometers within a local or meso-scale region is required to capture small-scale variations in aerosols for the accurate validation of satellite observations and to compare in situ versus remote sensing observations (Xiao et al., 2016; Holben et al., 2017). The MODIS (Moderate Resolution Imaging Spectroradiometer) retrieval AOD has a high accuracy with a wide spectral coverage (Tanré et al., 1997; Kaufman, et al. 1997) and the algorithm has been validated and improved based on AERONET data (Chu et al., 2002; Ichoku et al., 2002; Remer et al., 2005; Levy et al., 2010). Levy et al. (2013) refined the MODIS Collection 6 (C6) aerosol retrieval process to provide more accurate AOD retrievals. Some validations of satellite aerosol retrievals have been carried out in China with ground-based observations from CSHNET (Li, et al., 2007; Wang, et al., 2007; Xin, et al., 2007) and CARSNET (Che et al., 2009a, 2011a; Tao et al., 2015).

We investigated the variation in the optical properties of aerosols and aerosol radiative forcing (ARF) using three-minute intervals of sunphotometer measurements from 2011 to 2015 at seven adjacent CARSNET (~10–40 km) urban, suburban and rural sites over eastern China. The aims of this study were: (1) to investigate the synchronous variations and differences in the optical properties of aerosols over urban, suburban and rural areas of the YRD megacity, eastern China; (2) to analyze the type and dominant distribution pattern of aerosols in the YRD via the extinction and absorption properties of aerosols; (3) to understand the difference in the ARF calculated from ground-based measurements of the optical properties of aerosols over urban, suburban and rural areas in eastern China; and (4) to evaluate the MODIS AOD retrieval data using the CARSNET AOD for the YRD. The results of this study will help the satellite and modeling communities to improve future aerosol retrieval data and simulations.

2. Site descriptions, measurements and data

Fig. 1 shows the geographical locations of the seven CARSNET sites in the YRD; these locations are described in Table 1.

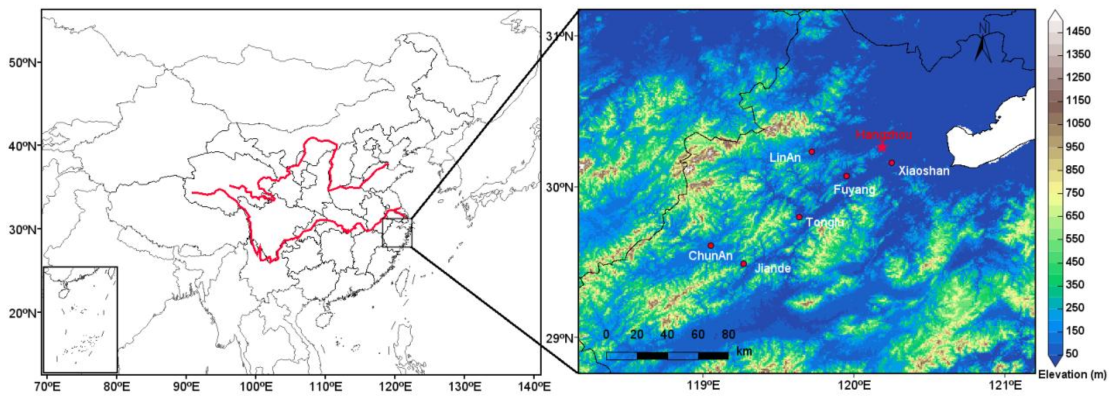

Fig.1. Geographical location and elevation map for the seven CARSNET sites in the YRD.

The rural site of ChunAn can be regarded as a representative clean site less affected by local and regional pollution. The site has a small population and a good ecological environment, although there is some agricultural activity and burning of biomass from crop residues. Hangzhou is a densely populated urban site with a large volume of vehicular traffic and is therefore more affected by anthropogenic activity. LinAn, Fuyang, Jiande, Xiaoshan and Tonglu are suburban sites and are all affected by both anthropogenic activity and pollution from industrial and agricultural production.

CE-318 sun photometers (Cimel Electronique, Paris, France) were installed at these seven sites in the YRD from 2011 to 2015. The instruments were standardized and calibrated annually according to the protocols reported by Che et al. (2009a). The instruments in this study were made inter-comparison calibration by the CARSNET reference instruments, which were periodically calibrated at Izaña in Spain. The cloud-screened AOD at different wavelengths was obtained using ASTPwin software (Cimel Electronique) (Smirnov et al.,2000). Instantaneous AOD measurements more than ten times at each day were selected for daily average calculation and statistical analysis to increase the representability of the aerosol optical characteristics (Che et al., 2015). The large AOD were checked by MODerate-resolution Imaging Spectroradiometer (MODIS) images (http://modis-atmos.gsfc.nasa.gov/IMAGES/) to further determine the cloud contamination. The corresponding values of Angström exponent (α) were calculated by instantaneous AOD values at 440 and 870 nm. The aerosol microphysical properties of the volume size distribution and aerosol optical properties—including the single-scattering albedo (SSA), the complex refractive index, the absorption AOD (AAOD), the absorption Angström exponent (AAE) and the fraction of spherical particles—were retrieved from the almucantar irradiance measurements according to the methods of Dubovik and King (2000) and Dubovik et al. (2002, 2006). The inversion algorithm is under an assumption of homogeneous nonsphericity aerosol particles distribution according to Dubovik (2006) and has been applied in many different types of areas world widely. The accuracies of SSA is~0.03, and the errors are about 30%–50%/0.04 for the imaginary/real part of the complex refractive index under the conditions of AOD at 440nm larger than 0.4 with the solar zenith angle more than 50°. The SSA was retrieved using only AOD_{440nm}>0.40 measurements to avoid the large uncertainties inherent in a low AOD (Dubovik et al. 2002, 2006). Real and imaginary parts of refractive index at 4 wavelengths (440, 675, 870, and 1020 nm) were retrieved from sky radiance and were confined in the range of 1.33–1.60 and 0.0005–0.50, respectively (Dubovik and King, 2000; Che et al., 2015b). Also retrieved were aerosol volumes of 22 size bins within the 0.05 - 15 um radius range. The EAOD in this study has been defined as extinction aerosol optical depth, and the AAOD and the AAE were calculated as described in equations (1) and (2):

$$AAOD(\lambda) = [1 - SSA(\lambda)] \times EAOD(\lambda) \quad (1)$$

$$AAE = -d\ln[AAOD(\lambda)]/d\ln(\lambda) \quad (2)$$

The ARF (aerosol radiative forcing) data were calculated by the radiative transfer module used by the AERONET inversion (García et al., 2012) under the assumption of cloud-free consideration. In this code, the aerosol vertical properties have been considered into a homogeneous atmosphere layers because of the weak dependent of ground radiances on the whole atmospheric column with minor uncertainties (Dubovik et al., 2000). The fluxes from 0.20 to 4.0μm were calculated according to the radiative transfer model GAME (Global Atmospheric ModEl) (Dubuisson et al., 1996, 2006; Roger et al., 2006). While the broadband radiation was calculated based on the aerosol optical depth, single scattering albedo and asymmetry factor based on those properties at four distinct wavelengths (440, 670, 870, 1020) which were linearly interpolated and extrapolated from the retrieval of the sun/sky-radiometer measurements. The uncertainties have been found to about 30% including the influence of spectral and solar zenith angle in the aerosol radiative effect (Myhre et al., 2003; Zhou et al., 2005). The size distribution, complex refractive index, and spherical particles fraction has been retrieved from the almucantar plane in the measurements. The SA (surface albedo) is obtained from the MODIS albedo product (MCD43C3) with the interpolation value of 440, 670, 870, and 1020 nm. The water vapor at 940 nm has been retrieved by the sun photometer. The ozone content was obtained from NASA Total Ozone Mapping Spectrometer measurements from 1978 to 2004. And other atmospheric gaseous data came from the US standard 1976 atmosphere model. In this study, the two parameters of ARF at the surface (ARF-BOA) and at the top of the atmosphere (ARF-TOA) have been calculated to describe the aerosol direct radiation effect to account for the changes of the solar radiation by calculating the difference energy between the aerosols presentation and absentation.

The MODIS C6 aerosol optical thickness products refined by Levy et al. (2013) were evaluated against our ground-based observations by the Deep Blue (at 10km) and Dark Target (at 3km and 10km) methods separately. This version of MODIS includes some important changes from earlier versions—such as the central wavelength assumptions, Rayleigh scattering and the gas absorption performance (Levy et al., 2013)—and improvements in the radiometric calibration (Lyapustin et al., 2014). All cloud- and snow-free land surfaces have been expanded in the MODIS C6 aerosol products (Hsu et al., 2013). The AOD averaged data from Terra-MODIS and Aqua-MODIS were validated by matching the averaged CARSNET AODs within 30 minutes of the MODIS overpass within the 5×5 pixels surrounding the CARSNET site (Tao et al., 2015). The AOD at 550 nm was interpolated between two wavelengths of the ground-based AOD measurements at 440 and 675 nm.

3. Results and discussion

3.1 Aerosol microphysical properties of radius and volume size distributions

Fig.2 shows the monthly aerosol size distribution (d*V*/dln*r*) in the YRD for all sites. The volumes of fine-mode aerosols were obviously higher than those of coarse-mode aerosols over all sites. The fine-mode radii were ~0.2–0.3 μm in the YRD with a volume fraction of 0.10–0.12 μm^3 and the coarse-mode radii were ~2.0 μm with a volume fraction close to 0.07 μm^3. The amount of fine-mode aerosols was higher in June and September than in other months at almost sites, except for Xiaoshan. This could be caused by aerosol humidification (Eck et al., 2012; Li et al., 2010, 2014; Huang et al., 2016). This phenomenon is also found over Beijing and Shenyang in north/northeast China, suggesting that hygroscopic growth occurs over many regions of China (Li et al., 2011; Che et al., 2015c).

The coarse-mode radius in spring at all sites was smaller than in other cities in north and northeast China affected by frequent dust transport events in spring (Kong et al., 2011; Zhao et al., 2015). The coarse-mode particles showed a larger effective radius at all seven urban, suburban and rural sites in the summer, which may due to the adhesion of new particles onto larger particles (such as fly ash).

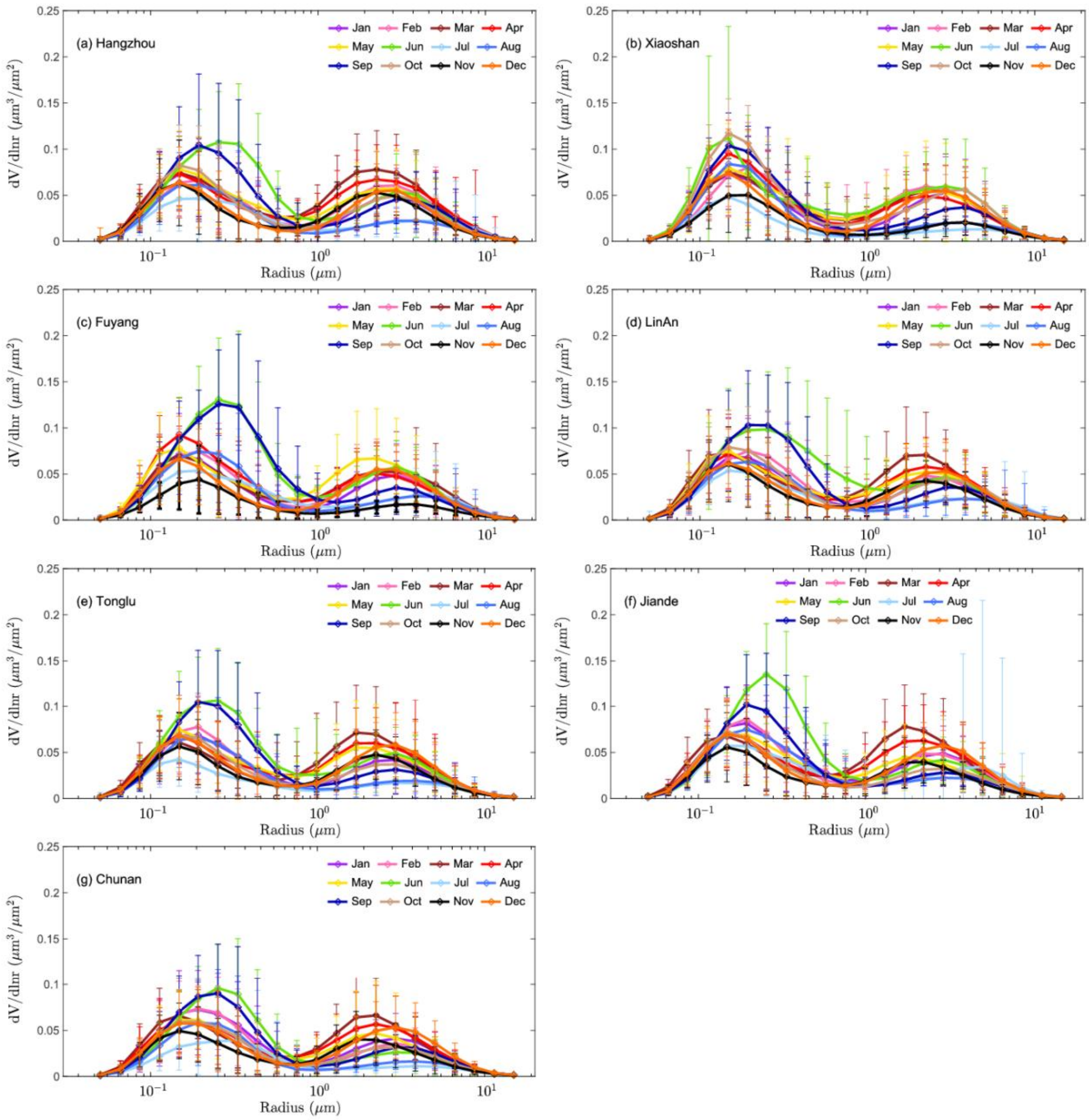

Fig.2.Variation in the annual volume size distribution over (a) Hangzhou, (b) Xiaoshan, (c) Fuyang, (d) LinAn, (e) Tonglu, (f) Jiande and (g) ChunAn.

3.2 Aerosol optical properties of Aerosol optical depth and Angström exponent

The annual mean of AOD at 440nm over the seven urban, suburban and rural sites in this study ranges from 0.68 to 0.76 (Table 1). Smaller observation sample has been found in Xiaoshan and Fuyang with 180 and 217 available observation days, respectively. The number of 180 observation days in Xiaoshan is less than half of the year may have less representative and need further data accumulation, while the observation days of 217 in Fuyang was more than half of the year may not affect the comparability between the other sites. The annual values of the AOD_{440nm} at Hangzhou, Xiaoshan, Fuyang, LinAn, Tonglu, Jiande and ChunAn were about 0.76±0.42, 0.76±0.43, 0.76±0.45, 0.73±0.44, 0.71±0.41, 0.73±0.40 and 0.68±0.38, respectively, which suggests that column aerosol loading is at a high level at all seven urban, suburban and rural sites in the YRD on the regional rather than the local scale. The AOD_{440nm} decreased from the eastern coast to the inland areas towards the west (from ~0.76±0.42 at Hangzhou to ~0.68±0.38 at ChunAn) due to the high aerosol loading from economic development and anthropogenic influences. The annual AOD_{440nm} shows that the aerosol loading has similar level in Hangzhou, Xiaoshan and Fuyang, and with the 4%-10% decrease in LinAn, Tonglu, Jiande and ChunAn, respectively. The AOD_{440nm} at the urban site of Hangzhou was higher as a result of the more industrial activity and high resident density in the eastern part metropolis region resulting in larger aerosol emissions compared with the other suburban and rural sites.

Table1.Geographical location and annual mean optical parameters of aerosols at the seven observation sites in the YRD.

	Hangzhou	Xiaoshan	Fuyang	LinAn	Tonglu	Jiande	ChunAn
Site type	Urban	Suburban	Suburban	Suburban	Suburban	Suburban	Rural
Longitude (°E)	120.19	120.25	119.95	119.72	119.64	119.27	119.05
Latitude (°N)	30.26	30.16	30.07	30.23	29.80	29.49	29.61
Altitude (m)	41.9	14.0	17.0	139	46.1	88.9	171.4
[a]N_{day}	485	180	217	562	498	480	439
[b]$N_{inst.}$	2052	752	906	2410	2255	1952	1731
[c]AOD_{500nm}	0.68±0.46	0.67±0.43	0.66±0.43	0.60±0.42	0.60±0.41	0.63±0.38	0.53±0.35
[d]AOD_{440nm}	0.76±0.42	0.76±0.43	0.76±0.45	0.73±0.44	0.71±0.41	0.73±0.40	0.68±0.38
[d]$AOD_{fine(440nm)}$	0.68±0.42	0.69±0.41	0.69±0.44	0.66±0.43	0.64±0.41	0.66±0.40	0.61±0.38
[d]$AOD_{coarse(440nm)}$	0.08±0.06	0.07±0.06	0.07±0.06	0.07±0.07	0.07±0.06	0.07±0.07	0.06±0.05
[e]EAE	1.29±0.26	1.37±0.24	1.32±0.24	1.29±0.27	1.30±0.26	1.32±0.28	1.22±0.25
[d]SSA_{440nm}	0.91±0.06	0.93±0.04	0.94±0.04	0.93±0.05	0.92±0.04	0.92±0.05	0.94±0.03
[f]SSA_{670nm}	0.92±0.06	0.91±0.06	0.93±0.06	0.92±0.05	0.93±0.05	0.92±0.07	0.94±0.03
[g]SSA_{870nm}	0.90±0.07	0.90±0.07	0.91±0.08	0.91±0.06	0.91±0.06	0.90±0.08	0.93±0.04
[h]SSA_{1020nm}	0.89±0.08	0.89±0.08	0.89±0.09	0.90±0.07	0.90±0.07	0.90±0.09	0.92±0.05
[d]Real	1.43±0.07	1.41±0.06	1.41±0.06	1.42±0.06	1.43±0.06	1.41±0.05	1.41±0.05
[d]Imaginary	0.011±0.010	0.008±0.006	0.007±0.006	0.009±0.007	0.009±0.007	0.010±0.009	0.007±0.004
[d]AAOD	0.06±0.05	0.05±0.04	0.04±0.04	0.05±0.04	0.05±0.04	0.06±0.04	0.04±0.03
[e]AAE	1.13±0.46	0.88±0.42	0.85±0.43	0.98±0.35	1.11±0.49	1.16±0.44	0.93±0.31
[d]$Rmeas_{t}$(μm)	0.70±0.34	0.65±0.31	0.66±0.33	0.66±0.33	0.65±0.33	0.62±0.24	0.65±0.30
[d]$Rmea_{fine}$(μm)	0.18±0.05	0.18±0.04	0.19±0.05	0.19±0.05	0.19±0.05	0.19±0.05	0.20±0.05

[d]Rmea$_{coarse}$(μm)	2.67±0.47	2.73±0.42	2.75±0.45	2.71±0.52	2.66±0.48	2.63±0.47	2.74±0.49
[d]Reff(μm)	0.30±0.10	0.29±0.09	0.30±0.09	0.29±0.10	0.29±0.10	0.29±0.09	0.30±0.10
[d]Reff$_{fine}$(μm)	0.16±0.04	0.16±0.03	0.17±0.04	0.16±0.04	0.16±0.04	0.17±0.04	0.17±0.04
[d]Reff$_{coarse}$(μm)	2.21±0.40	2.26±0.35	2.30±0.39	2.24±0.44	2.19±0.41	2.16±0.39	2.27±0.42
[d]Volume(μm^3)	0.19±0.09	0.19±0.09	0.19±0.09	0.18±0.09	0.17±0.09	0.18±0.09	0.17±0.07
[d]Volume$_{fine}$(μm^3)	0.10±0.06	0.11±0.06	0.11±0.07	0.10±0.06	0.10±0.06	0.10±0.06	0.10±0.06
[d]Volume$_{coarse}$(μm^3)	0.09±0.06	0.08±0.05	0.08±0.06	0.08±0.05	0.08±0.06	0.08±0.07	0.07±0.05
[d]ARF-BOT(W/m^2)	−93±44	−84±41	−80±40	−81±39	−79±39	−82±40	−74±34
[d]ARF-TOA(W/m^2)	−35±20	−36±21	−37±21	−36±21	−35±20	−35±21	−40±19

[a] Number of available observation days.
[b] Number of instantaneous observations.
[c] Optical parameters at a wavelength of 500nm.
[d] Optical parameters at a wavelength of 440 nm.
[e]Angström exponents between 440 and 870 nm.
[f] Optical parameters at a wavelength of 670 nm.
[g] Optical parameters at a wavelength of 870 nm.
[h] Optical parameters at a wavelength of 1020 nm.

Ding et al. (2013a,b) showed that plumes from agricultural burning in June may significantly and seriously affect the radiation balance and air quality of the YRD region. In this study, the monthly averaged AODs at most sites showed two peaks in June and September (Fig.3) with values of ~1.26±0.50 and ~1.03±0.57, respectively. This may be attributed to the accumulation of fine-mode particles via hygroscopic growth in the summer season and the burning of crop residue biomass under a continental high-pressure system with good atmospheric stability and frequent temperature inversions. These conditions lead to the poor diffusion of pollutants (Xia et al., 2007). As Fig.3 shown, the monthly average value of the extinction Angström exponent (EAE, $-d\ln[EAOD(\lambda)]/d\ln(\lambda)$) in Hangzhou was higher in January (~1.40±0.23) and September (~1.43±0.24). This conclusion is also indicated the dominance of small particles from anthropogenic emissions and agricultural activity in autumn and winter (Tan et al., 2009).

The annual fine-mode AOD values at Hangzhou, Xiaoshan, Fuyang, LinAn, Tonglu, Jiande and ChunAn were about 0.68±0.42, 0.69±0.41, 0.69±0.44, 0.66±0.43, 0.64±0.41, 0.66±0.40 and 0.61±0.38, respectively (Fig.3). The seasonal variation in the AOD was similar to the total AOD at these urban, suburban and rural sites. The fine-mode fraction of AOD consistently exceeded 0.90 which indicates a major contribution of fine mode fraction to the total AOD in the YRD. Moreover, the figure 3 shows that the EAE at Hangzhou, Xiaoshan, Fuyang, LinAn, Tonglu, Jiande and ChunAn was about 1.29±0.26, 1.37±0.24, 1.32±0.24, 1.29±0.27, 1.30±0.26, 1.32±0.28 and 1.22±0.25, respectively. Values of EAE >1.20 were found in all months throughout the year, indicating that small particle size distributions were favored in the YRD region. The annual coarse-mode AOD values at Hangzhou, Xiaoshan, Fuyang, LinAn, Tonglu, Jiande and ChunAn were between about 0.06 and 0.08 with the coarse mode fraction of AOD about 0.10 which indicates the 10% contribution of coarse mode fraction to the AOD in the YRD. The less coarse mode fraction indicated that there is no obvious effect of the coarse particles in the YRD region than that contributed to the higher aerosol loading in other north/northeast China (Zhang et al., 2012). Some dusts cases can be observed in YRD region that transported from north/northwest China during 2012-2015 reflect the effect of mineral dust aerosols (Gong et al., 2003). The fugitive dust from road traffic and construction activity is another more persistent and significant source for China’s cities as well as these eastern megacities.

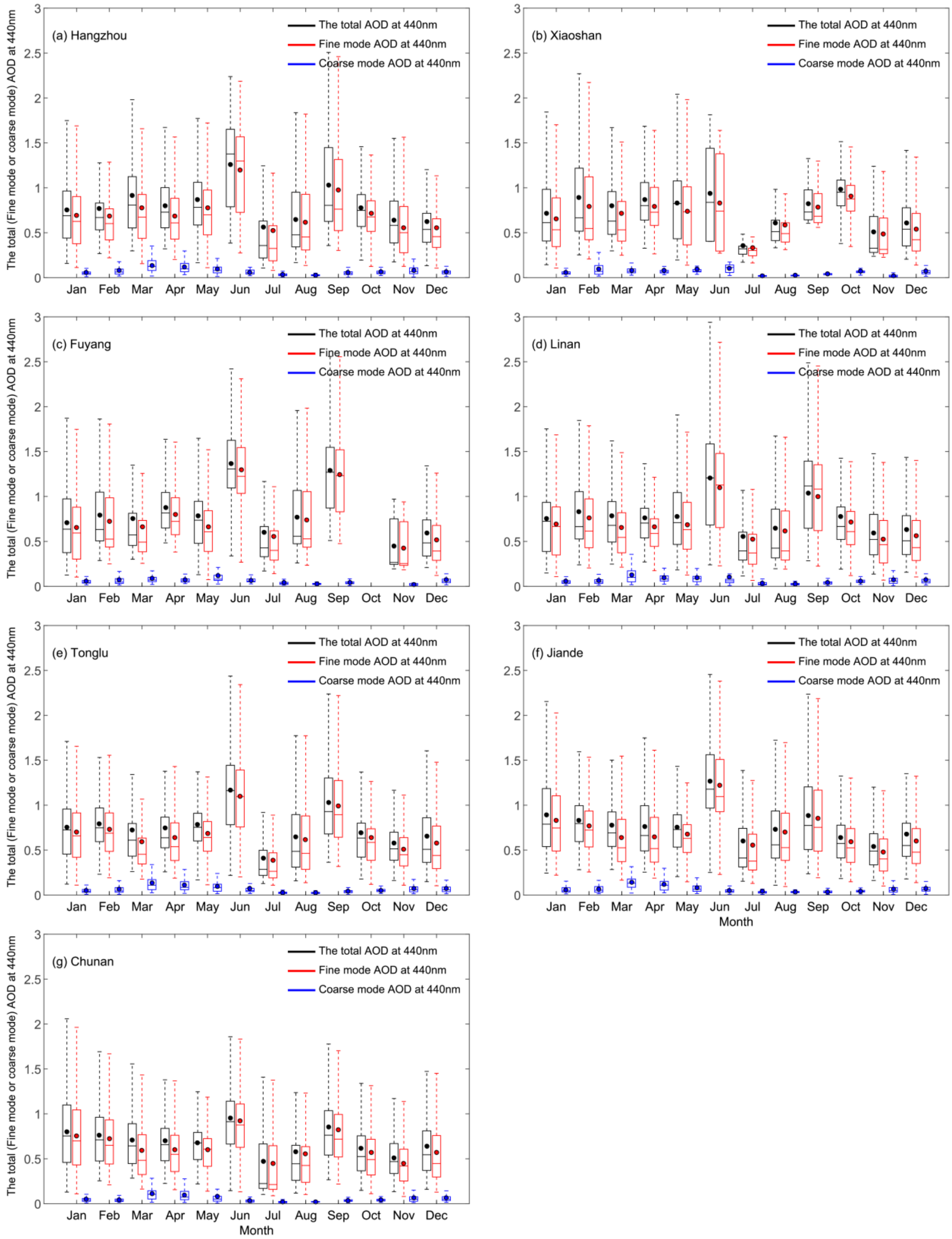

Fig. 3. Variation in the total, fine- and coarse-mode AOD$_{440\ nm}$ over (a) Hangzhou, (b) Xiaoshan, (c) Fuyang, (d) LinAn, (e) Tonglu, (f) Jiande and (g) ChunAn. The boxes represent the 25th to 75th percentile distribution, while the dots and solid lines within each box represent the mean and median, respectively.

The monthly and diurnal cycle of AOD at 500nm has also been discussed in Fig.4 and Fig.5. The annual values of AOD500nm over the seven urban, suburban and rural sites in this study varied from 0.53 (ChunAn) to 0.68 (Hangzhou).The results show that two peaks of AOD at 500nm occurs in June and September with values of 1.25±0.59 and 1.00±0.42 in the urban site of Hangzhou, respectively which has the similar pattern as the other sites. The increase of AOD at 500nm in June is not corresponding to the same increase pattern of EAE (about 1.5) which indicates the aerosols types may be relatively constant in this region. The Fig.5 depicts the diurnal patterns of AOD at 500nm in this megacity area of eastern China. We can see that there are two types of diurnal patterns in this region. The daily AOD has been found increased in early morning (08:00 hr to 09:00 hr) and afternoon (12:00 hr to 14:00 hr) about the value of 0.60 to 0.70in Hangzhou, Xiaoshan, Fuyang and Linan, while the decreasing of daily AOD has been observed from 0.70 to 0.50 during the daytime (from 07:00 hr to 16:00 hr) in Tonglu, Jiande and ChunAn. The high AOD during 07:00～09:00 in the urban area may be due to the anthropogenic activities and aerosol emissions from the morning rush hour. The decreased AOD with the value of 0.37±0.36 occurred in the suburban cities of Tonglu, Jiande and ChunAn may be due to the meteorological conditions more than anthropogenic effects. During the day, the aerosols in the near-surface may spread into vertical as a result of turbulence due to the more and more unstable atmosphere by the continuous strengthening of solar radiation.

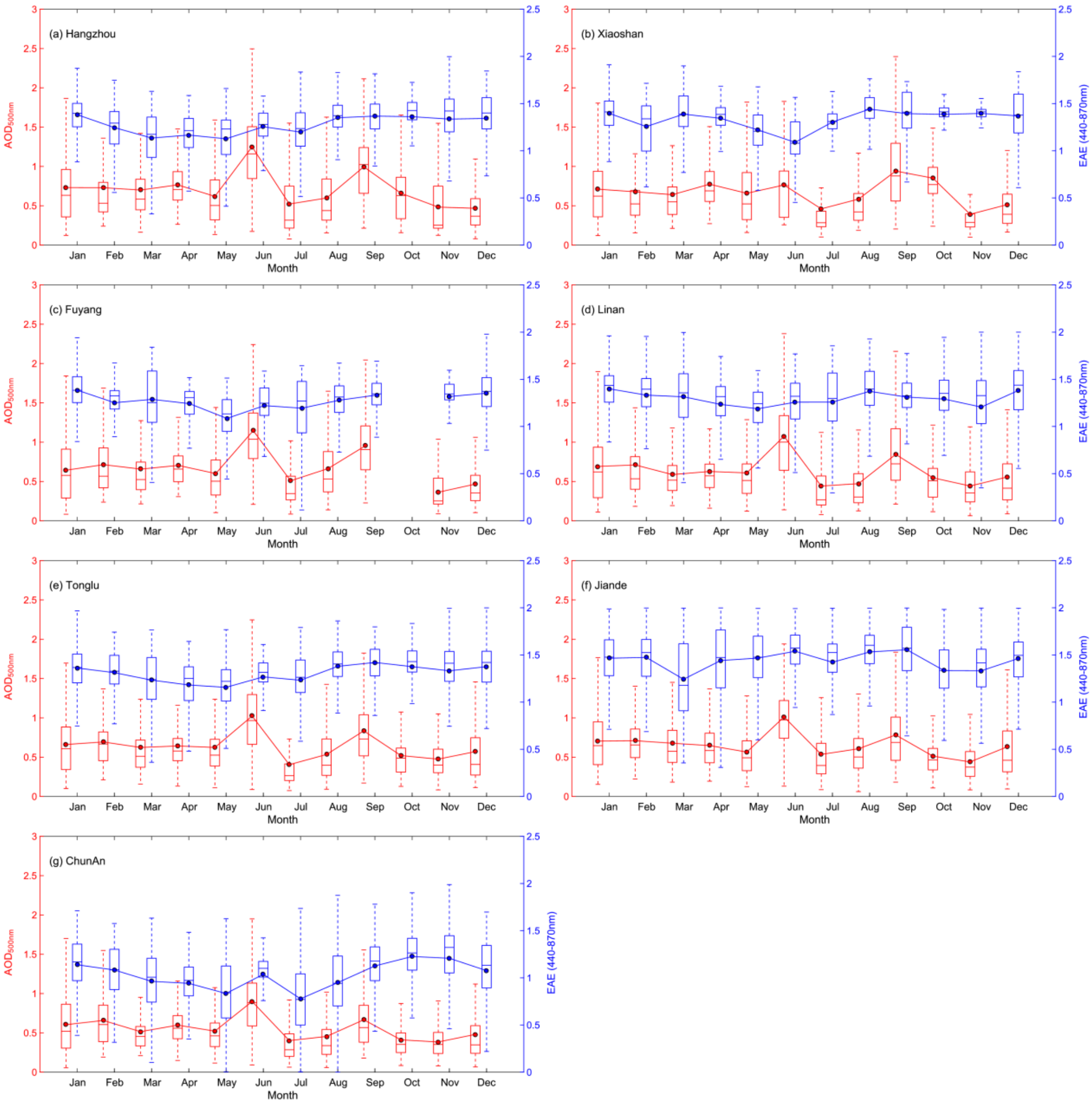

Fig.4.Variation in the AOD at 500nm & EAE at 440–870 nm over (a) Hangzhou, (b) Xiaoshan, (c) Fuyang, (d) LinAn, (e) Tonglu, (f) Jiande and (g) ChunAn. The boxes represent the 25th to 75th percentile distribution, while the dots and solid lines within each box represent the mean and median, respectively.

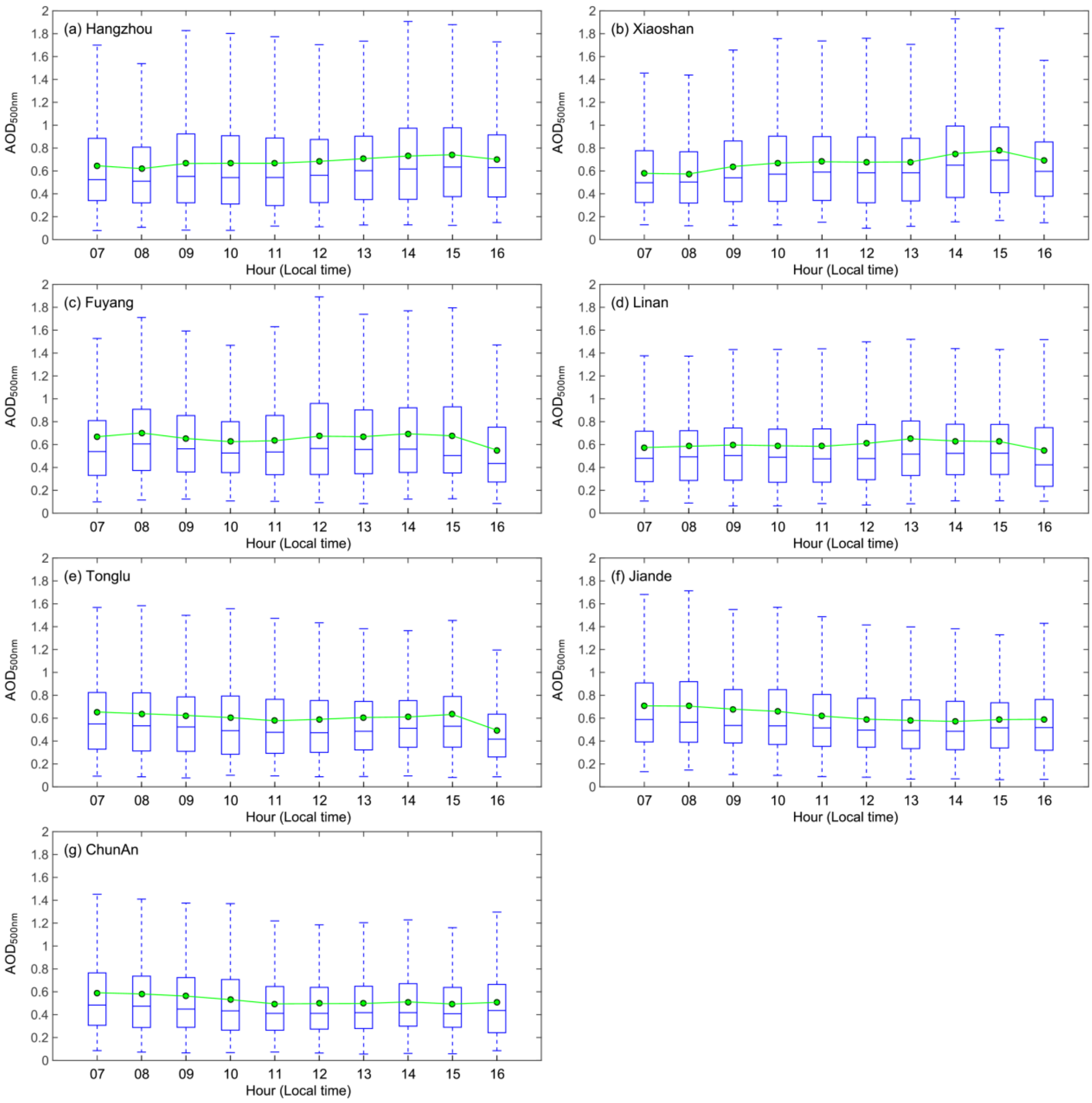

Fig.5. Variation of diurnal cycle in the AOD at 500 nm over (a) Hangzhou, (b) Xiaoshan, (c) Fuyang, (d) LinAn, (e) Tonglu, (f) Jiande and (g) ChunAn. The boxes represent the 25th to 75th percentile distribution, while the dots and solid lines within each box represent the mean and median, respectively.

The product of MODIS/Terra and MODIS/Aqua with Deep Blue (at 10km) and Dark Target (at 3km and 10km) methods has been evaluated against by ground-based observations separately in Fig. 6-8. We use the better estimated data of Quality flag = 3 and Quality flag=2, 3 for DT and TB methods, respectively. The systematic performance of the MODIS/Terra C6 retrieval AOD values was generally more stable in the YRD region compared with the MODIS/Aqua product with the two Deep Blue and Dark Target methods, which most of the plots scattered around the 1:1 regression line.

The correlation coefficients (R) between the MODIS/Aqua and MODIS/Terra between by the Dark Target methods at 3km and sun photometer AOD (550 nm) values were about 0.84 to 0.92 and 0.85 to 0.94 in the YRD region, respectively. The linear regression fitting performed better at the suburban sites of LinAn and Jiande according to the product of MODIS/Terra by the Dark Target methods at 3km. The fitting curve was almost consistent with the 1:1 reference line, which suggests that the aerosol properties were well defined for the MODIS C6 products. A large part of the MODIS retrieval AOD value was outside the expected error envelope of ±($0.05 + 20\%\tau_{CARSNET}$), especially for AOD values<0.80 in Hangzhou and Xiaoshan. This indicates that the MODIS retrieval algorithm could still be improved, especially in urban areas. The MODIS retrieval AOD performed better at the other five sites (Fuyang, LinAn, Tonglu, Jiande and ChunAn) in the YRD; most of the retrieved AOD values for these sites fell within the expected error envelope. The MODIS/Aqua retrievals with Dark Target methods at 3km were underestimated while the MODIS/Terra retrievals with Dark Target methods at 3km were overestimated except Hangzhou, Tonglu and Jiande. The small deviation at the suburban sites suggested that the MODIS C6 retrieval using the DT method was suitable for capturing the optical properties of aerosols in suburban areas with dense vegetation coverage of the YRD. However, this method may have larger difference in the urban areas with less vegetation such as Hangzhou. The correlation coefficients (R) of the MODIS/Aqua and MODIS/Terra between sun photometer AOD (550 nm) values by the Deep Blue and Dark Target methods at 10km were about 0.81 to 0.90, 0.85 to 0.90, 0.69 to 0.91 and 0.85 to 0.93 in the YRD region, respectively. The MODIS/Aqua and MODIS/Terra retrievals with Deep Blue and Dark Target methods at 10km were underestimated except Hangzhou and Xiaoshan. In particular, the biases of the correlation coefficients (R) occurred in LinAn and Jiande has decreased from 0.94 and 0.90 to 0.87 and 0.88. The validation results indicate a good MODIS/Terra matching with better fitting correlation at 3km rather than 10km products.

The AOD overestimation retrieved using Dark Target (DT) and Deep Blue (DB) methods are more influenced by the SSA and the phase function of aerosol in eastern China with AOD >0.4

(Tao et al. 2015). Therefore, the detailed ground-based observation in this work is more helpful to the calibration of MODIS retrievals in eastern China.

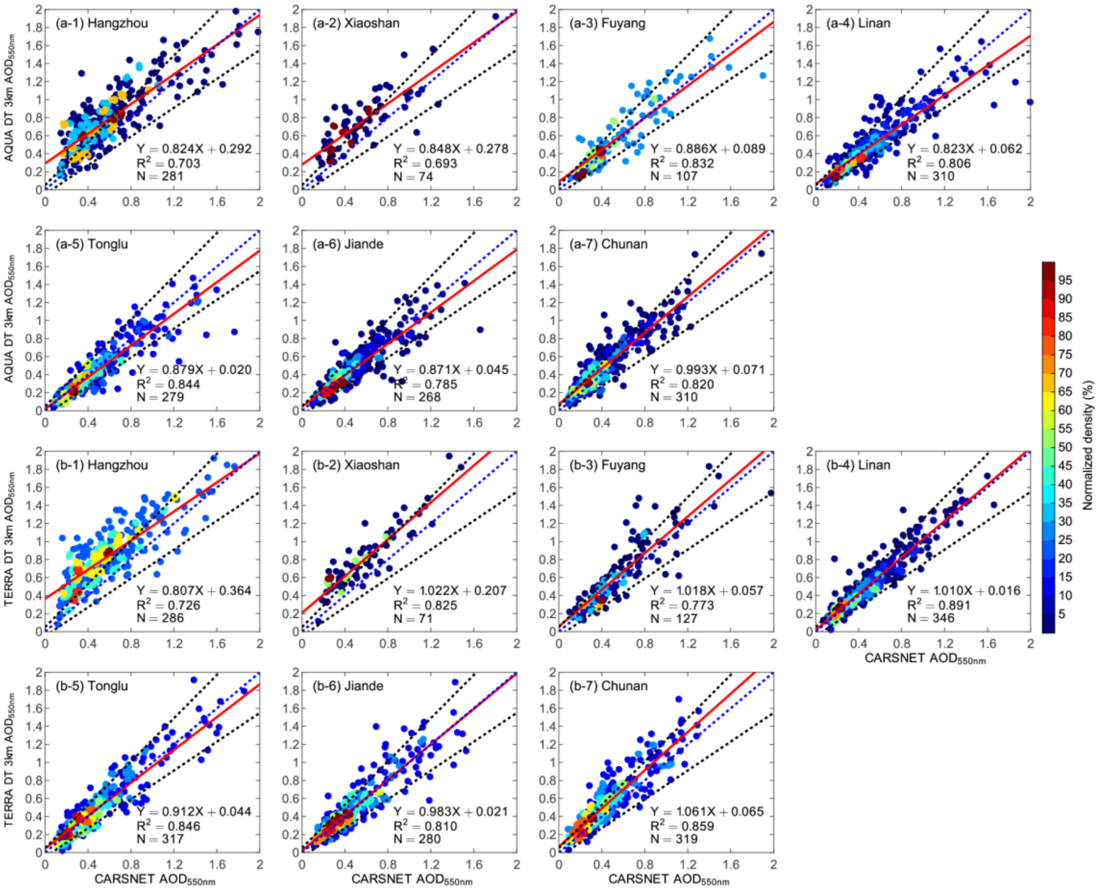

Fig.6. Comparison of MODIS/Aqua Dark Target (DT) AOD at 550 nm with the CARSNET AOD at 3km in (a-1) Hangzhou, (a-2) Xiaoshan, (a-3) Fuyang, (a-4) LinAn, (a-5) Tonglu, (a-6) Jiande, (a-7) ChunAn and MODIS/Terra DT AOD at 550 nm with the CARSNET AOD at 3km in (b-1) Hangzhou, (b-2) Xiaoshan, (b-3) Fuyang, (b-4) LinAn, (b-5) Tonglu, (b-6) Jiande, (b-7) ChunAn. The red solid line represents the linear regression. The two black dotted lines represent the expected errors in the MODIS retrievals.

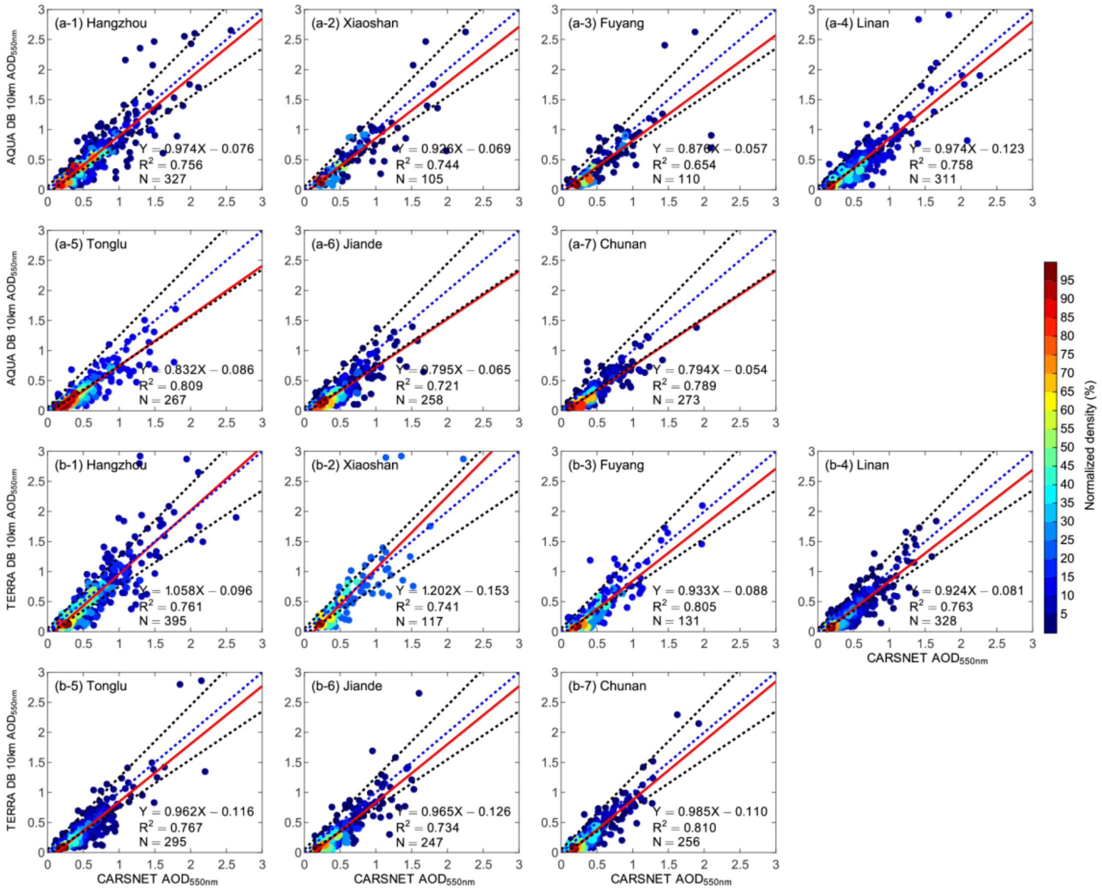

Fig.7. Comparison of MODIS/Aqua Deep Blue (DB) AOD at 550 nm with the CARSNET AOD at 10km in (a-1) Hangzhou, (a-2) Xiaoshan, (a-3) Fuyang, (a-4) LinAn, (a-5) Tonglu, (a-6) Jiande, (a-7) ChunAn and MODIS/Terra AOD DB at 550 nm with the CARSNET AOD at 10km in (b-1) Hangzhou, (b-2) Xiaoshan, (b-3) Fuyang, (b-4) LinAn, (b-5) Tonglu, (b-6) Jiande, (b-7) ChunAn. The red solid line represents the linear regression. The two black dotted lines represent the expected errors in the MODIS retrievals.

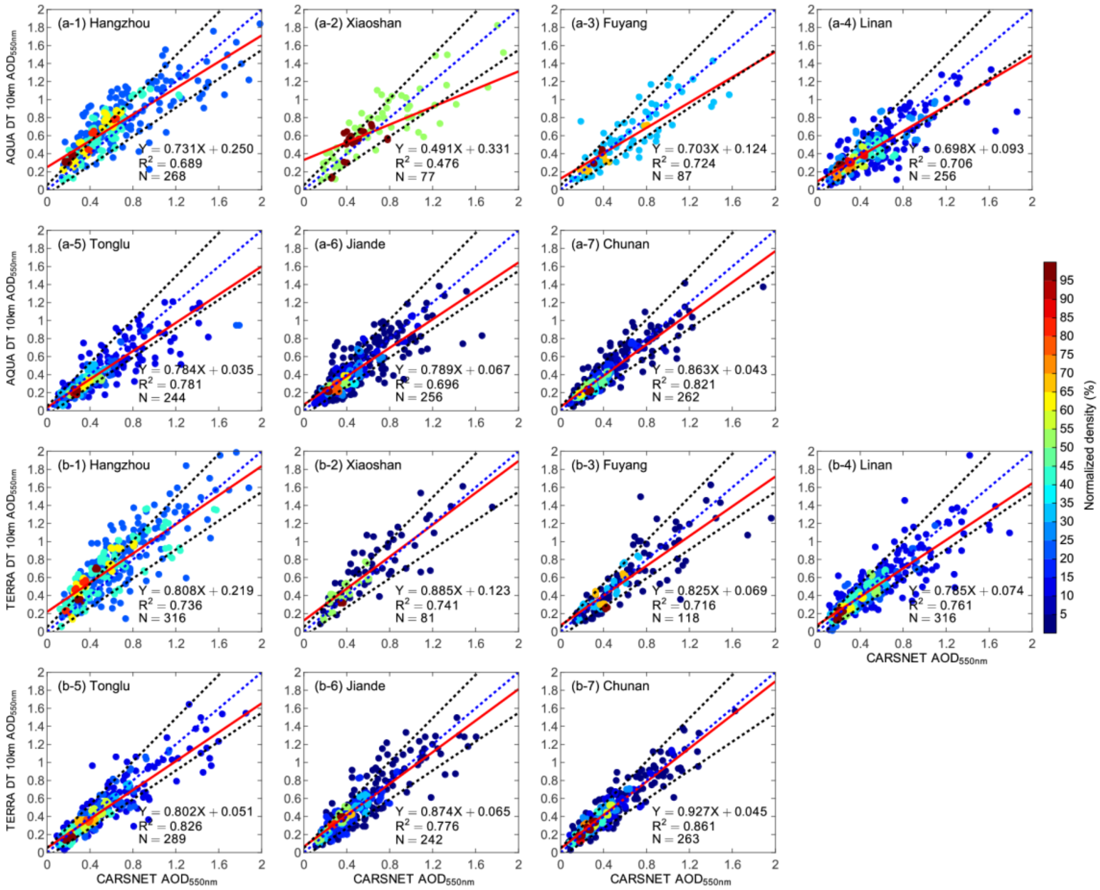

Fig.8. Comparison of MODIS/Aqua AOD DT at 550 nm with the CARSNET AOD at 10km in (a-1) Hangzhou, (a-2) Xiaoshan, (a-3) Fuyang, (a-4) LinAn, (a-5) Tonglu, (a-6) Jiande, (a-7) ChunAn and MODIS/Terra DT AOD at 550 nm with the CARSNET AOD at 10km in (b-1) Hangzhou, (b-2) Xiaoshan, (b-3) Fuyang, (b-4) LinAn, (b-5) Tonglu, (b-6) Jiande, (b-7) ChunAn. The red solid line represents the linear regression. The two black dotted lines represent the expected errors in the MODIS retrievals.

The relationship between the EAE and the spectral difference in the EAE ($\delta EAE = EAE_{440–675nm} - EAE_{675–870nm}$) was analyzed to investigate the contribution of fine particles (R_f) and their fraction (η) to the total extinction (EAOD) at 440 nm (Gobbi et al., 2007). In this framework, values of AOD>0.15 are represented by different colors to avoid errors in the δEAE. The lines indicate contribution of the fixed radius (R_f) and fraction (η) of the fine-mode particles to the total extinction. Gobbi et al. (2007) used the difference in the EAE and AOD data to determine the growth of fine-mode particles or contamination by coarse-mode particles at eight AERONET stations: Beijing (China), Rome (Italy), Kanpur

(India), Ispra (Italy), Mexico City (Mexico), NASA Goddard Space Flight Center (GSFC, USA), Mongu (Zambia) and Alta Floresta (Brazil).

Fig.9 shows that the high EAOD values (>1.00) cluster in the plots for all seven urban, suburban and rural sites, which is attributed to fine-mode particles with δEAE<0 and *η* ~50–90%. This variation in the fine-mode particles is similar to the results from Beijing and Kanpur (*η* ~70–90%). However, there were very few coarse-mode particles (δEAE~0, *η*~0–10%) in this study, suggesting that the dominance of dust is not significant in eastern China. These results showed a different pattern from that of other regions in north/northeast China (Wang et al., 2010; Zhu et al., 2014). For δEAE~0 and 10%<*η*<30%, high extinction was associated with a mixture dominated by fine-mode particles and less persistent coarse-mode particles. Clustering concentrated in the region α∼1.5, δα ∼−0.5 with high AOD values at all sites, which may be linked to an increase in size of the fine-mode particles by coagulation as the aged and hygroscopic events, as seen at other locations (e.g. Ispra, Italy; Mexico City, Mexico; GSFC, USA).

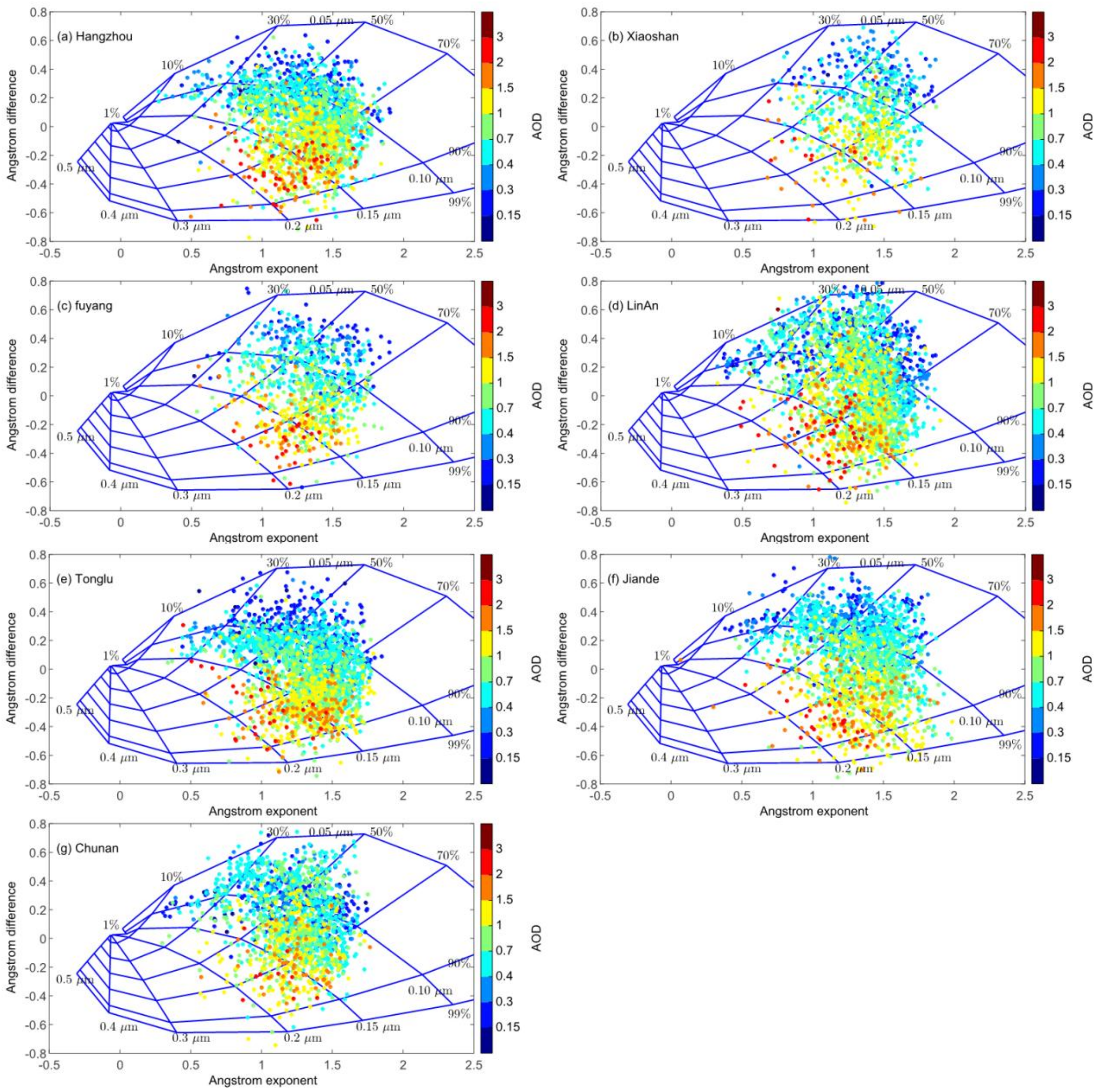

Fig.9. Angström exponent difference as a function of $\alpha_{440–870\ nm}$ and the $AOD_{440\ nm}$ over (a) Hangzhou, (b) Xiaoshan, (c) Fuyang, (d), LinAn, (e) Tonglu, (f) Jiande and (g) ChunAn.

3.3 Aerosol optical properties of single-scattering albedo and aerosol complex refractive index

The distribution of the SSA at the wavelengths of 440nm, 670nm, 870nm and 1020nm over the seven sites in the YRD are shown in Fig.10. The SSA varied from 0.91 to 0.94, which is similar to the range seen in other regions of China, such as Wuhan (0.92), Beijing (0.89) and Xinglong (0.92) (Wang et al., 2015; Xin et al., 2014; Zhu et al., 2014). This indicated that scattering aerosol particles in eastern China resulting from high levels of industrial and anthropogenic activity were dominant. The characteristics of the SSA at these seven sites gradually increased from the east coast (0.91±0.06 at Hangzhou) inland toward the west (0.94±0.03 at ChunAn). The seven observation sites may always controlled by the same weather system that indicates a weak effect of meteorological elements in each site to the change of aerosol optical characteristics. These results indicate the emissions caused by human activity affect the absorption of aerosols in urban areas. The SSA was higher at LinAn and ChunAn than at the other sites, which may reflect the presence of a larger number of scattering aerosols (e.g. particles from urban/industrial activities) over the clean rural sites than over urban or suburban sites.

The SSA over urban and suburban sites showed the largest monthly variation. The monthly average values of SSAT were high in February (~0.94±0.05) and June (~0.92±0.06), but low in March (~0.90±0.06) and August (~0.89±0.09) in Hangzhou. However, the monthly SSA values at the rural site of ChunAn only varied from 0.92 to 0.95. We concluded that the type of aerosol at urban/suburban sites was more complex than at rural sites. The increased level of scattering aerosols with higher SSA in June may be influenced by the hygroscopic growth in favor of the interaction between aerosols from different emissions sources (Xia et al., 2007). The existence of light-absorbing dust aerosols may contribute to the weaker lower SSA in spring while the aerosols from biomass burning were probably due to the strong decreased in SSA values in August (Yang et al., 2009).

The wavelength dependence of SSA present specific absorption/scattering properties of different type aerosol (Sokolik and Toon, 1999; Eck et al., 2010). The SSA of dust in spring shown a dependence on the spectrum from 440nm to 1020nm in general (Cheng et al., 2006; Dubovik et al., 2002). Especially in March, the SSA at 440nm in Hangzhou, LinAn, Jiande and ChunAn was obviously lower at short wavelength than that in the longer wavelength. This result has shown a strong absorption of dust in the short wavelength in the YRD region over eastern China. It's worth noting that there is an obvious and strong decreasing of SSA in the longer wavelength of aerosol from biomass burning or industrial emissions in August. The wavelength dependence of SSA in YRD could be used to simply describe the aerosol types including dust or the biomass burning smoke.

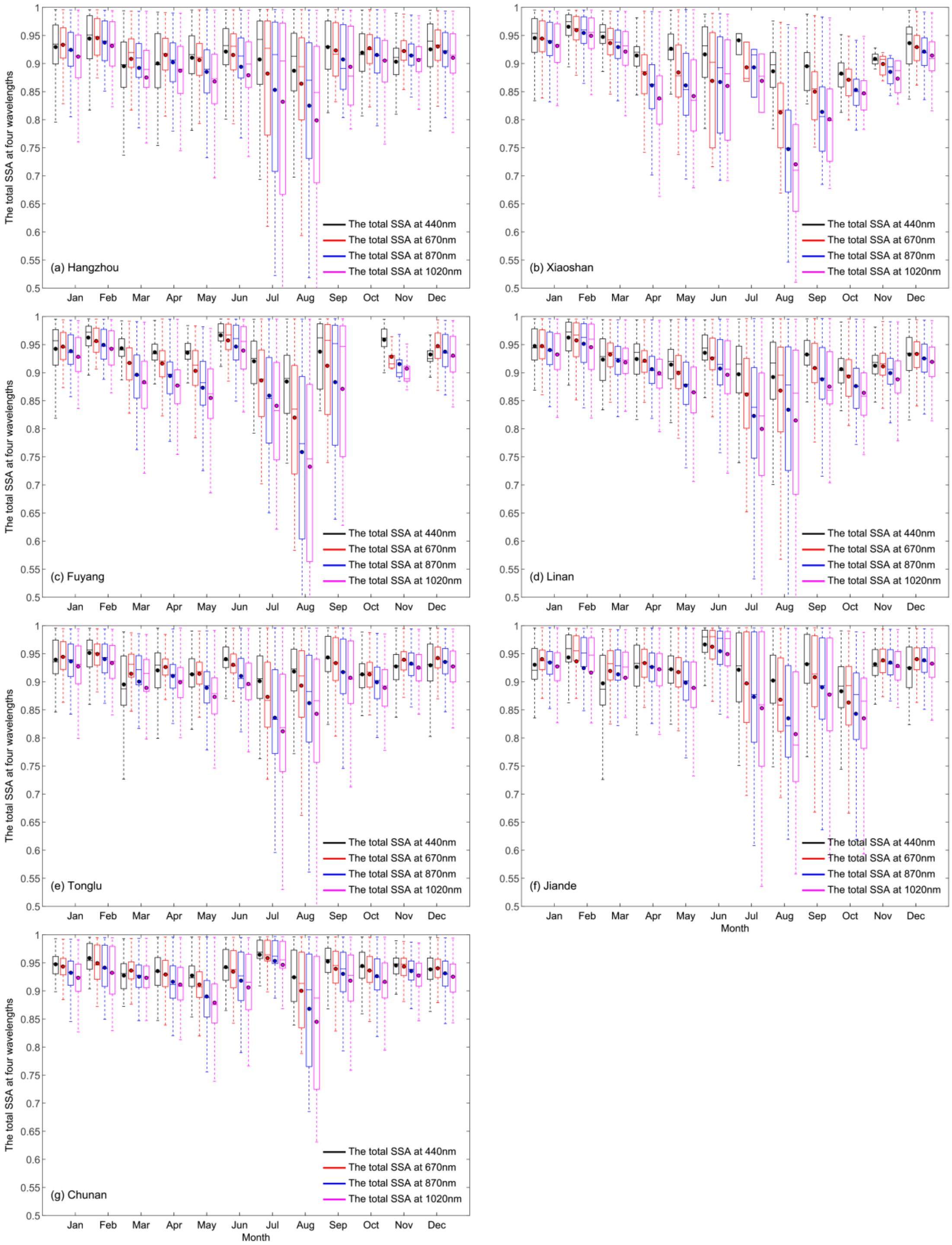

Fig.10. Variation in the SSA at 440nm, 670nm 870nm and 1020nmover (a) Hangzhou, (b) Xiaoshan, (c) Fuyang, (d) LinAn, (e) Tonglu, (f) Jiande and (g) ChunAn. The boxes represent the 25th to 75th percentile distribution, while the dots and solid lines within each box represent the mean and median, respectively.

The real and imaginary parts of the refractive index represent the scattering and absorption capacity of particles, respectively. The refractive index is determined by the hygroscopic conditions and the chemical composition of the aerosols (Dubovikand King, 2000). There was no significant difference between the real parts of the refractive index among the seven urban, suburban and rural sites in this study (range 1.41–1.43). The real parts of the refractive index in this study were smaller than the real parts of ammonium sulfate and ammonium nitrate (1.55), which may be due to the hygroscopic conditions or the mixture of dust particles. The real part of the refractive index was highest in March (~1.46±0.06) and November (~1.45±0.06) and lowest in July (~1.42±0.06) and August (~1.41±0.07) at the urban sites.

The imaginary part of the refractive index was higher at the urban site of Hangzhou (~0.0112 ± 0.0104) as a result of the high loading of absorption aerosols in this region and was consistent with the lower SSA. High imaginary parts of the refractive index occurred in August at all urban, suburban and rural sites in the YRD, which may be due to the higher emission of absorptive particles by the post-harvest burning of crop residues with more spectral dependence. The burning of crop residues may cause a large deterioration in the regional air quality in the YRD region. A higher level of spring dust aerosols with absorption could contribute to a higher value of the imaginary part of the refractive index.**3.4 Aerosol optical properties of absorption aerosol optical depth and absorption Angström exponent**

The annual AAODs at Hangzhou, Xiaoshan, Fuyang, LinAn, Tonglu, Jiande and ChunAn were about 0.06±0.05, 0.05±0.04, 0.04±0.04, 0.05±0.04, 0.05±0.04, 0.06±0.04 and 0.04±0.03, respectively (Fig.11). The similar AAOD level at the seven sites (0.04-0.06) suggests that absorbing aerosols are distributed homogeneously in the YRD region. The AAOD values may have very large an uncertainty because of the dataset is including all the values in one month. Nevertheless, there is also some varies in AAOD according to the changes of the SSA in section 3.3. These differences in the AAOD were mostly dependent on the type of aerosol and the ratio of absorbing and non-absorbing components in the aerosols.

The monthly AAOD at the urban site of Hangzhou was 0.09±0.06 in March as a result of the presence of absorbing dust particles. The AAOD of about 0.07±0.04 in August is related to the burning of crop residues. The AAODs in the winter season at all the sites in the YRD region were <0.05, which suggests that absorbing aerosol emissions did not frequently occur at these sites, unlike in the northern regions of China. As fig.12 shown, the AAE was<1.00 in June and August at all urban, suburban and rural sites of the YRD, which suggested the presence aerosols coated with absorbing or non-absorbing material in summer season. This process is favored by high temperatures and high humidity under conditions of strong solar radiation (Shen et al., 2015, Zhang et al., 2015). The particles coagulate and grow rapidly in the presence of sufficient water vapor (Li et al., 2016). The AAE became increasingly close to, or larger than, 1.00 at all seven sites from September, which is consistent with decreasing amounts of precipitation. This increase in the AAE was related to the emission of black carbon from biomass burning (Soni et al., 2010; Russell et al., 2010). According to the corresponding annual mean values for the AAE at Hangzhou, Xiaoshan, Fuyang, LinAn, Tonglu, Jiande and ChunAn (1.13±0.46, 0.88±0.42, 0.85±0.43, 0.98±0.35, 1.11±0.49, 1.16±0.44 and 0.93±0.31) in Fig. 12, the seven sites has been attributed to three categories with AAE levels. The mean values of the AAE at Xiaoshan and Fuyang were <1.00, suggesting the presence of absorbing or non-absorbing materials coating black carbon at these suburban and rural sites (Bergstrom et al., 2007; Lack and Cappa et al., 2010; Gyawali et al., 2009). The AAE values were close to 1.00 at LinAn and ChunAn, indicating that the absorptive aerosols were dominated by particles of black carbon (Zhang et al., 2012; Li et al., 2016). By contrast, the AAE values at Hangzhou, Tonglu and Jiande were >1.00, indicating the presence of absorptive aerosols from the burning of biomass. This difference in the AAE distribution indicates the absorbing aerosols have different characteristics resulting from the different emission sources at urban, suburban and rural sites in the YRD.

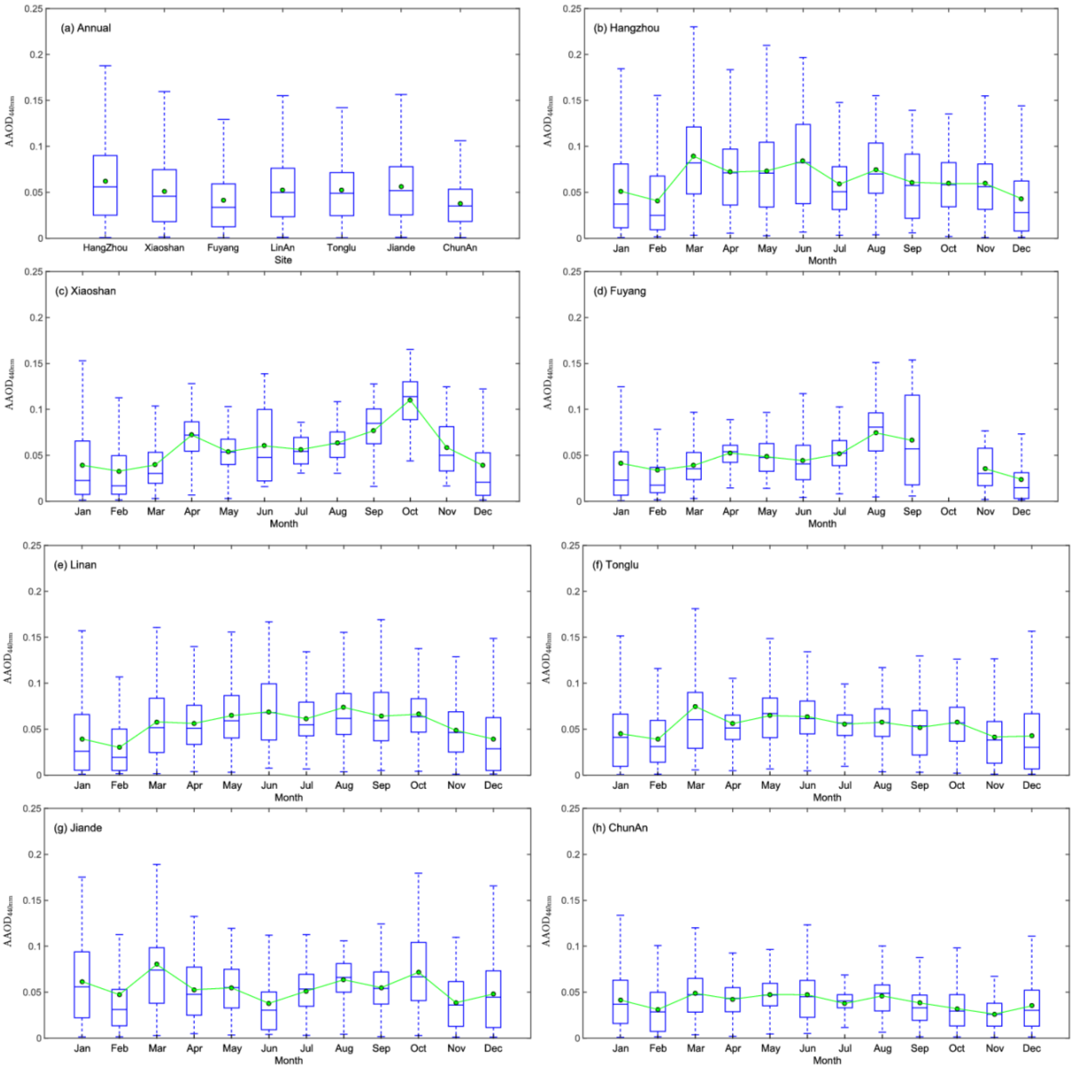

Fig.11. (a) Annual variation in the absorption aerosol optical depth at 440 nm ($AAOD_{440\ nm}$) over (b) Hangzhou, (c) Xiaoshan, (d) Fuyang, (e) LinAn, (f) Tonglu, (g) Jiande and (h) ChunAn. The boxes represent the 25th to 75th percentile distribution, while the dots and solid lines within each box represent the mean and median, respectively.

The AAE can be used to indicate the major types (urban/industrial, biomass burning, dust/mixed dust) or optical mixtures of absorbing aerosol particles (Schnaiter et al., 2006; Russellet al., 2010; Giles et al., 2011; 2012; Mishra and Shibata, 2012). Giles et al., (2011) examined AAE/EAE data from Kanpur to classify the categories of absorbing aerosols. The "mostly dust" category has been defined as having an EAE value ≤0.50 and sphericity fraction <0.20 with an AAE value>2.00. The "mostly black carbon" category has been defined as having an EAE value>0.80 and a sphericity fraction ≥0.20 with 1.00<AAE≤2.00. Values of EAE>0.80 and AAE>2.00 indicate a concentration of organic carbon (Arola et al., 2011). The “mixed black carbon and dust” category was centered at EAE~0.50 with AAE~1.50and used to represent an optical mixture with black carbon and mineral dust particles as the dominant absorbers.

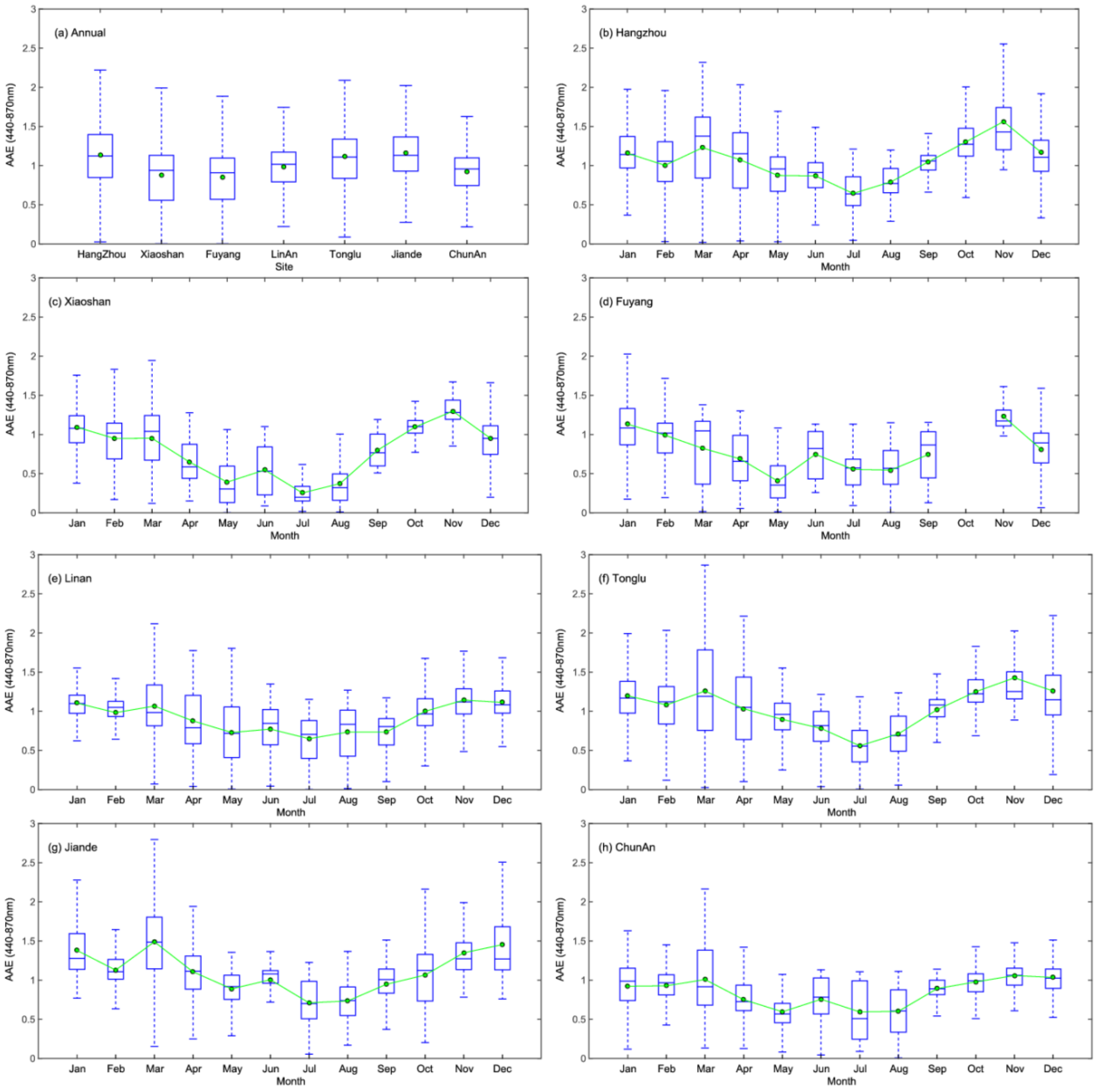

Fig.12. (a) Annual variation in the absorption Angström exponent at 440 nm ($AAE_{440\ nm}$) over (b) Hangzhou, (c) Xiaoshan, (d) Fuyang, (e) LinAn, (f) Tonglu, (g) Jiande and (h) ChunAn. The boxes represent the 25th to 75th percentile distribution, while the dots and solid lines within each box represent the mean and median, respectively.

We used the instantaneous AAE and EAE values to classify the dominant absorbing aerosol types in urban, suburban and rural areas of the YRD (Fig. 13). Fig. 13 shows that the "mostly dust" category was very low at both suburban and rural sites (<0.01%) and just ~0.24% at the urban site of Hangzhou. This indicates the YRD region is completely different from other north/northeast region in China where the dust particles could contribute to the aerosol loading substantially. The "mostly black carbon" category dominates the absorbing aerosols in the urban, suburban and rural areas in the YRD region. The percentage "mostly black carbon" varied from ~20 to 40% depending on each site, indicating the mixing of black carbon as well as brown and soot carbon species from biomass burning and urban/industrial activities. Because of the long-distance transportation and local fugitive dust effect, the "mixed black carbon and dust" category contributed~5% of the absorbing aerosol particles in the YRD region. There was also ~1-4% of the "organic carbon" category identified as absorbing aerosol particles in this region. The non-absorption particles are account for ~50 to 80% in the YRD region. There is higher contribution of non-absorption particles about 78.17% in Fuyang and less non-absorption particles about 50.01% in Jiande. The result is consistent with the level of total SSA at 440nm of Fuyang (0.94) with more scattering particles than Jiande (0.92). Particles with EAE values of ∼0.40 and ∼1.25 could be regarded as "mixed large particles" greater than microns in size and submicron "mixed small particles", respectively (Giles et al. 2012). The frequency of "mixed large particles" was <0.5% at the urban, suburban and rural sites. By contrast, the frequency of "mixed small particles" was ∼18-36%.

The EAE (α_{ext}) and AAE (α_{abs}) values at all the urban, suburban and rural sites were distributed mainly around 1.25 and 1.00–1.50, respectively (Fig.14). In contrast with the results of Giles et al. (2011), the sphericity fraction did not show an obvious transition from non-spherical to spherical particles from the urban, suburban and rural sites in YRD. The sphericity fraction showed a dispersed distribution of spherical particles, indicating a mixture of fine-mode particles derived from anthropogenic sources and coarse-mode particles, such as dust events transported from north/northwest China or local fugitive dust emissions.

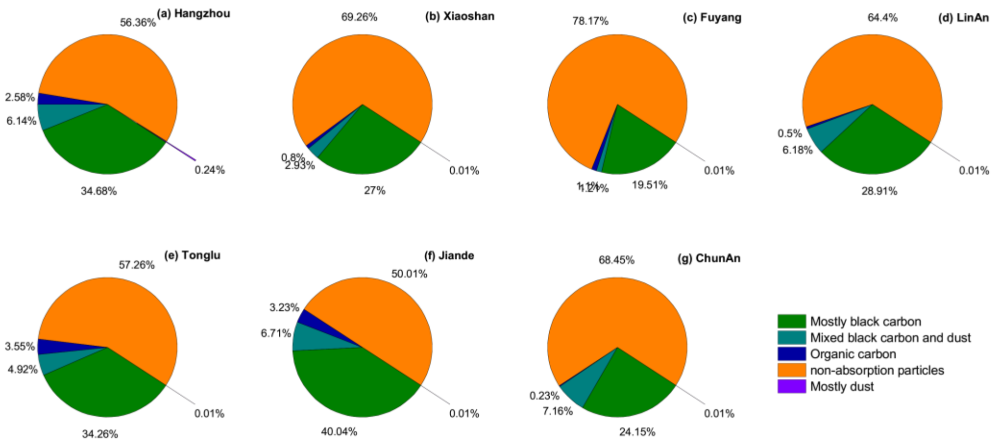

Fig.13.Types of aerosol over (a) Hangzhou, (b) Xiaoshan, (c) Fuyang, (d), LinAn, (e) Tonglu, (f) Jiande and (g) ChunAn.

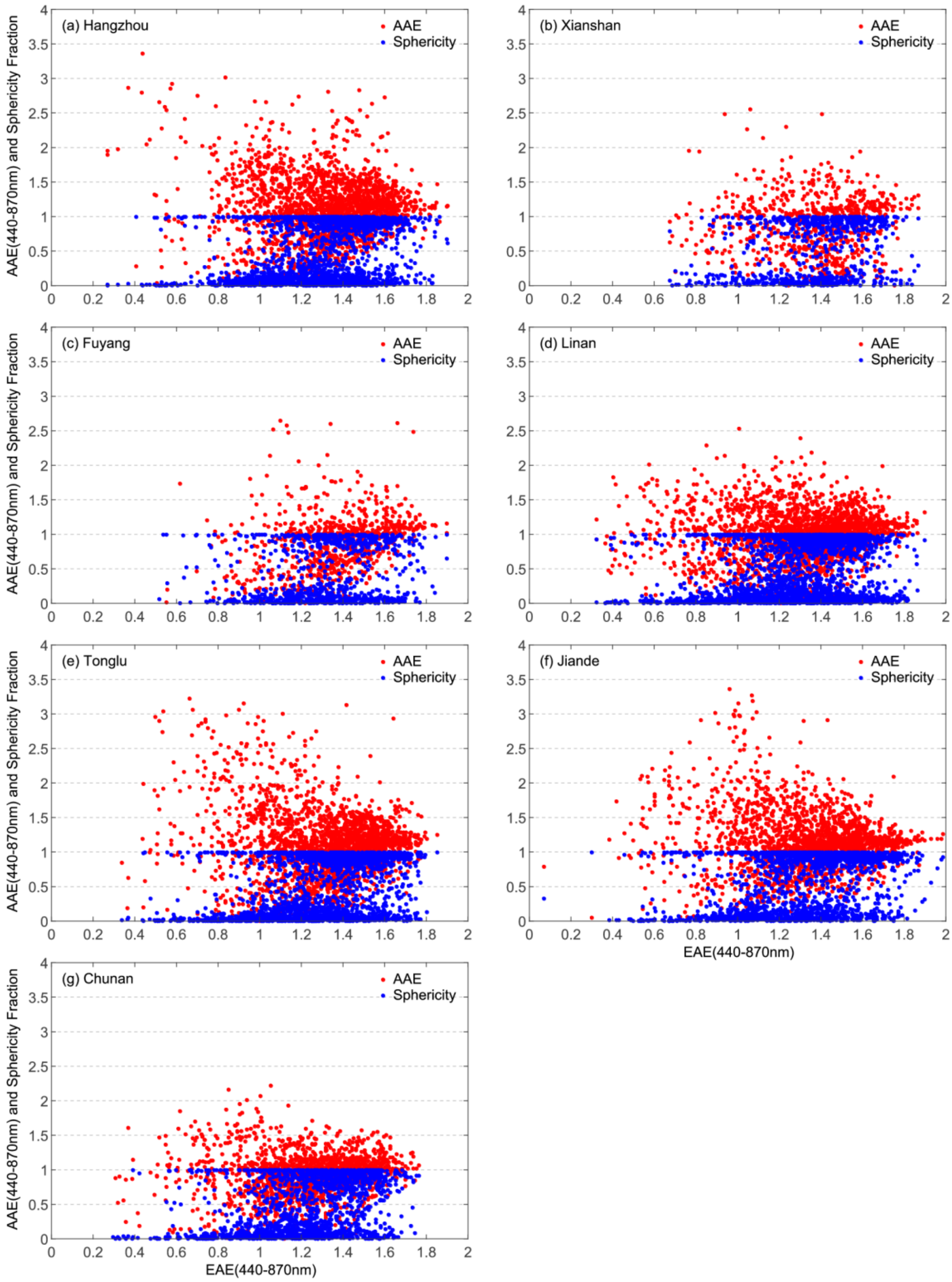

Fig.14.The AAE (red dot) and the sphericity fraction (blue dot) as a function of the EAE at 440–870 nm over (a) Hangzhou, (b) Xiaoshan, (c) Fuyang, (d), LinAn, (e) Tonglu, (f) Jiande and (g) ChunAn.

3.5 Aerosol optical properties of aerosol radiative forcing at the Earth's surface and top of the atmosphere

Figures 15 and 16 show the variations in ARF at the surface (ARF-BOA) and at the top of the atmosphere (ARF-TOA) at the urban, suburban and rural sites in the YRD region.

The annual ARF-BOA values for Hangzhou, Xiaoshan, Fuyang, LinAn, Tonglu, Jiande and ChunAn were about −93±44, −84±40, −80±40, −81±39, −79±39, −82±40 and −74±34W/m^2, respectively. The higher ARF-BOA values in Hangzhou indicate that there was high aerosol loading at this site, which scattered and absorbed more radiation and caused a significant cooling effect at the surface. The monthly value of the ARF-BOA in Hangzhou was higher in June (about −132±48 W/m^2) and September (about −106±48 W/m^2), which is consistent with the timing of burning biomass from crop residues. Ding et al. (2016) found that black carbon emitted from biomass burning can modify the meteorology of the planetary boundary layer and substantially decrease the surface heat flux. Hygroscopic grow that the same time enhances the aerosol optical extinction (Yan et al., 2009; Zhang et al., 2015); this was also an important factor in the large ARF-BOA values in June and September at the urban, suburban and rural sites in the YRD.

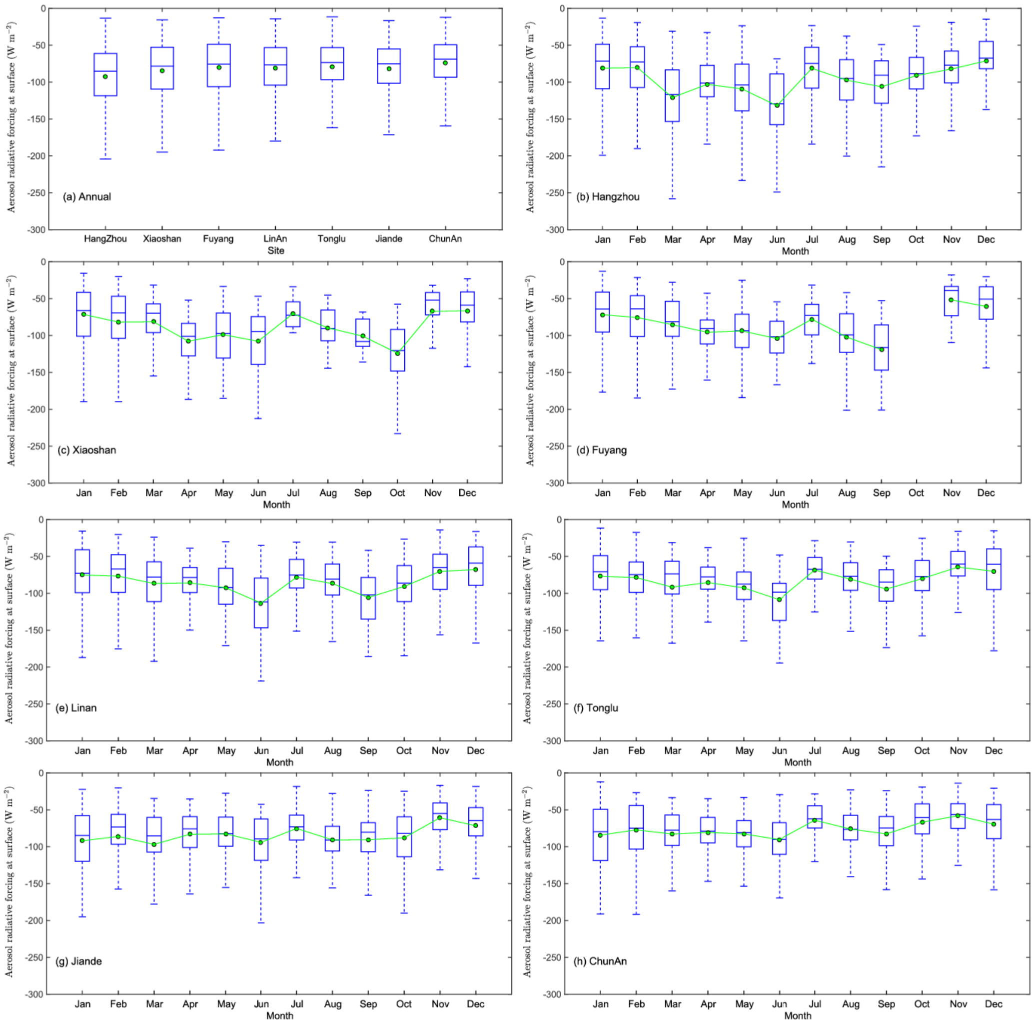

Fig.15.(a) Annual variation of the ARF at the surface over (b) Hangzhou, (c) Xiaoshan, (d) Fuyang, (e) LinAn, (f) Tonglu, (g) Jiande and (h) ChunAn. The boxes represent the 25th to 75th percentile distribution, while the dots and solid lines within each box represent the mean and median, respectively.

The ARF-TOA values were less than−40 W/m^2 at the urban, suburban and rural sites in the YRD. The AFR-TOA values were negative all year, which suggests that the aerosols caused a cooling effect at the TOA as well as at surface in the YRD. This is different from the north/northeast regions of China, where the instantaneous AFR-TOA value can be positive in the winter season as a result of the large surface reflectance on short wavelength radiation and heating caused by absorbing aerosols (Che et al., 2014). The surface albedo in the YRD region is lower than in north/northeast China as a result of better vegetation. At the same time, there is also a low level of absorbing aerosol emissions in winter. This caused obvious negative AFR at the TOA at the urban, suburban and rural sites in the YRD.

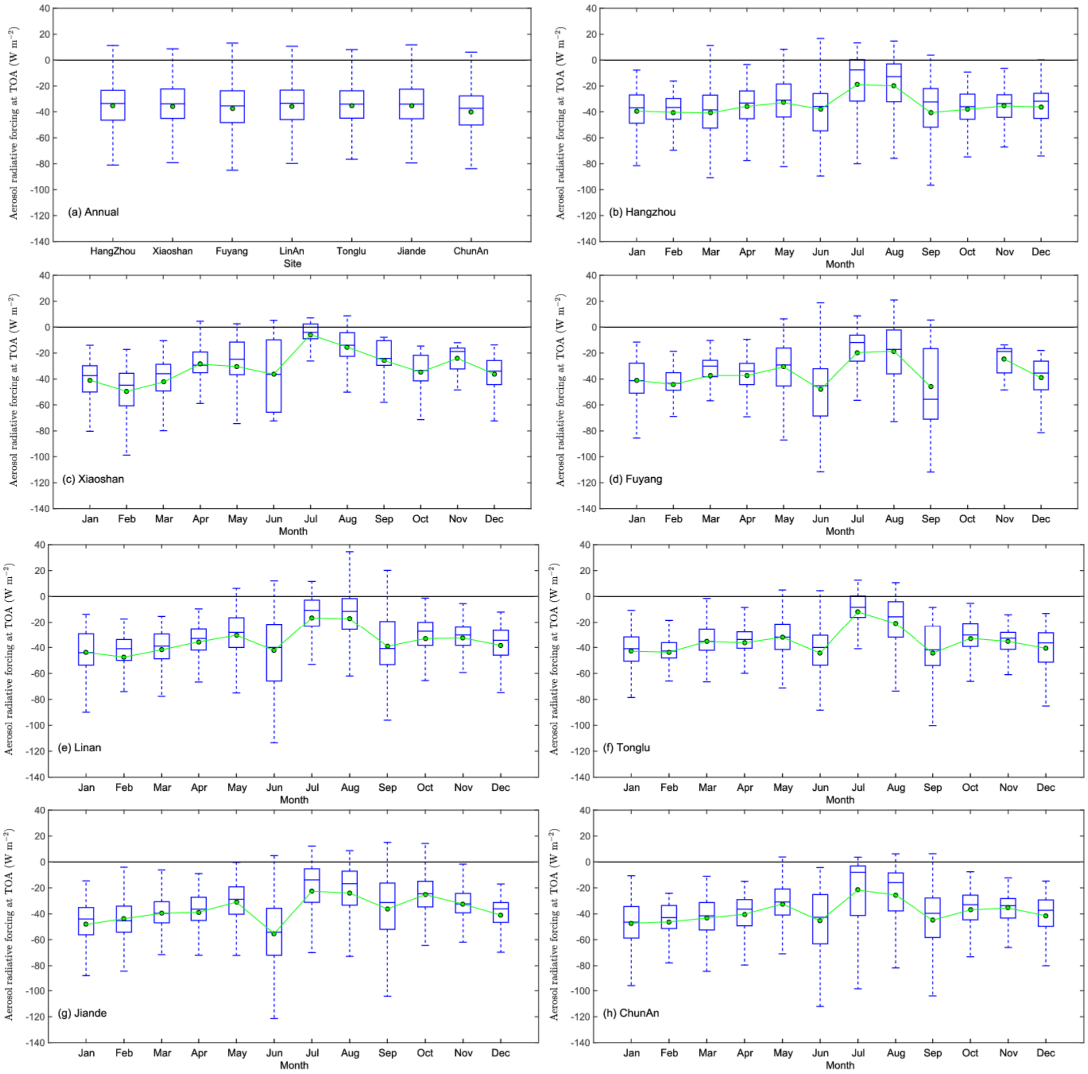

Fig.16. (a) Annual variation in the aerosol radiative forcing at the top of the atmosphere (TOA) in (b) Hangzhou, (c) Xiaoshan, (d) Fuyang, (e) LinAn, (f) Tonglu, (g) Jiande and (h) ChunAn. The boxes represent the 25th to 75th percentile distribution, while the dots and solid lines within each box represent the mean and median, respectively.

4. Discussion and Summary

In this paper, the aerosol optical properties, including the AOD, EAE,SSA, complex refractive index, volume size distribution, and the absorption properties of the AAOD and AAE were retrieved from ground-based measurements data over the YRD in eastern China for the period 2011–2015. The AOD in Hangzhou in urban eastern China was similar to that in Shenyang (0.75) in urban northeast China (Zhao et al., 2013), and in Beijing (0.76) and Tianjin (0.74) in urban north China (Che et al., 2015b), indicating that the aerosol extinction is both common and at a similar level throughout most urban areas of China. The AOD values at the urban and suburban sites of Hangzhou were slightly higher than at Pudong (0.70) and Hefei (0.69), other urban areas in eastern China, suggesting that higher aerosol extinction ability were observed here (He et al., 2012; Liu et al., 2017). However, the AOD at all seven sites was lower than that obtained at Wuhan (1.05), Nanjing (0.88), Dongtan (0.85), Taihu(0.77) and Xuzhou (0.92) in previous studies in eastern China (Wang et al., 2015; Li et al., 2015; Pan sphericity et al., 2010; Xia et al., 2007; Wu et al., 2016). This indicates that the aerosol loading caused by anthropogenic activities is very high in both urban and suburban areas in eastern China. The site at LinAn is regarded as the clean suburban site in eastern China with an average AOD about 0.73±0.44, which is higher than that at the other regional background stations of China, such as Longfengshan (0.35; northeastern China), Mt Waliguan (0.14, inland Asia), Xinglong (0.28, northern China), Akedala (0.20, northwestern China) and Shangri-La (0.11, southwestern China) (Wang et al., 2010; Che et al., 2011; Zhu et al., 2014; Che et al., 2015b). The aerosol loading in eastern China (especially in the YRD region) is at least twice as high as in other regions of China which indicate the strong aerosol extinction. Moreover, aerosol extinction was at a high level over both urban and suburban sites and even over the rural sites in the YRD which suggests large regional scale aerosol loading over eastern China in recent years.

The fine mode fraction of AOD (>0.90) and coarse mode fraction of AOD (~0.10) as well as the relationship between the EAE and the spectral difference in the EAE suggested the dominance of fine mode fraction to the AOD and the subordinate position of coarse mode fraction in the YRD. The validation results indicates a good Terra-MODIS matching with better fitting correlation at 3km rather than 10km products with the retrievals performed better in suburban than in urban and rural areas, but were systematically over estimated in rural and urban areas and their immediate surroundings.

The range of SSA at 440nm was about 0.91–0.94 in the YRD region which suggesting the presence of mainly scattering aerosol particles in eastern China as a result of high industrial and anthropogenic activity. The SSA of dust was weakly lower at short wavelength while the SSA of aerosol from biomass burning has the strong wavelength dependence in the longer wavelength.

The similar AAOD levels at the seven sites indicated that absorbing aerosols were homogeneously distributed in the YRD region. The difference in the distribution of the AAE suggests that the absorbing aerosols have different characteristics depending on the emission source. The "mostly black carbon" category was the dominant contributor of absorbing aerosols at the urban, suburban and rural sites in the YRD region. The submicron "mixed small particle" category had a significant effect on the aerosol optical properties over the YRD region. The sphericity fraction showed a dispersed distribution of spherical particles, indicating a mixture of both fine- and coarse-mode particles from anthropogenic and natural sources.

The large ARF-BOA indicated a high aerosol loading that scattered and absorbed more radiation with the stronger aerosol cooling effect at the surface in the YRD region. Both the burning of biomass from crop residues and the hygroscopic growth of particles could make important contributions to the ARF-BOA in summer over the YRD region. The AFR-TOA values were negative all year with an aerosol cooling effect at the TOA while the instantaneous positive in AFR-TOA value in the winter by the large surface reflectance of better vegetation has been found different from the north/northeast China.

The column aerosol optical properties over urban, suburban and rural areas of YRD region of China were investigated and the results will increase our understanding of the characteristics and sources of aerosol emissions over eastern China. Future research should consider the vertical distribution of aerosols by Lidar, the validation of the aerosol optical results of other satellite products such as VIIRS and GOCI, and a comprehensive analysis of the physical and chemical properties of aerosols and meteorological factors.

Acknowledgments

This work was supported by grant from National Key R & D Program Pilot Projects of China (2016YFA0601901), National Natural Science Foundation of China (41590874 &41375153), Natural Science Foundation of Zhejiang Province (LY16010006), the CAMS Basis Research Project (2016Z001 & 2014R17), the Climate Change Special Fund of CMA (CCSF201504), CAMS Basic Research Project (2014R17),the Special Project of Doctoral Research supported by Liaoning Provincial Meteorological Bureau (D201501), Hangzhou Science and Technology Innovative project (20150533B17)and the European Union Seventh Framework Programme (FP7/2007-2013) under grant agreement no. 262254.

Reference

Ackerman, P., and Toon, O.B.: Absorption of visible radiation in atmosphere containing mixtures of absorbing and nonabsorbing particles, Appl. Opt., 20, 3661-3668, 1981.

Albrecht, B.: Aerosols, cloud microphysics, and fractional cloudiness, Science, 245, 1227-1230, 1989.

Arola, A., Schuster, G.,Myhre, G.,Kazadzis, S.,Dey, S., and Tripathi, S. N.: Inferring absorbing organic carbon content from AERONETdata, Atmos. Chem. Phys., 11, 215–225, doi:10.5194/acp-11-215-2011, 2011.

Bergstrom, R.W., Pilewskie, P., Russell, P.B., Redemann, J., Bond, T.C., Quinn, P.K., and Sierau, B.: Spectral absorption properties of atmospheric aerosols, Atmos. Chem. Phys., 7, 5937–5943, doi: 10.5194/ acp-7-5937-2007, 2007.

Charlson, R.J., Schwartz, S.E., Hales, J.M., Cess, D., Coakley, J.A., and Hansen, J.E.: Climate forcing by anthropogenic aerosols, Science, 255, 423–430, 1992.

Che, H.Z., Xia, X.A., Zhu, J., Wang, H., Wang, Y.Q., Sun, J.Y., Zhang, X.C., Zhang, X.Y., and Shi, G.Y.: Aerosol optical properties under the condition of heavy haze over an urban site of Beijing, China, Environ. Sci. Pollut. Res., 22, 1043–1053, 2015a.

Che, H. Z., Zhang, X. Y., Alfraro, S., Chatenet, B., Gomes, L., and Zhao, J. Q.: Aerosol optical properties and its radiative forcing over Yulin, China in 2001 and 2002, Adv. Atmos. Sci., 26, 564–576, doi:10.1007/s00376-009-0564-4, 2009b.

Che, H., Zhang, X., Chen, H., Damiri, B., Goloub, P., Li, Z., Zhang, X., Wei, Y., Zhou, H., Dong, F., Li, D., and Zhou, T.: Instrument calibration and aerosol optical depth (AOD) validation of the China Aerosol Remote Sensing Network (CARSNET), J. Geophys. Res., 114, doi: org/10.1029/2008JD011030, 2009a.

Che, H., Yang, Z., Zhang, X., Zhu, C., Ma, Q., Zhou, H., and Wang, P.: Study on the aerosol optical properties and their relationship with aerosol chemical compositions over three regional background stations in China, Atmos. Environ., 43, 1093–1099, doi:10.1016/j.atmosenv.2008.11.010, 2009c.

Che, H., Wang, Y., Sun, J., and Zhang, X.: Assessment of In-situ Langley Calibration of CE-318 Sunphotometer Mt. Waliguan Observatory, China, SOLA, 7, 089-092, doi: 10.2151/sola.2011-023, 2011

Che, H., Wang, Y., and Sun, J.: Aerosol optical properties at Mt.Waliguan observatory, China, Atmos. Environ., 45, 6004–6009, 2011.

Che, H.Z., Zhang, X.Y., Xia, X.A., Goloub, P., Holben, B., Zhao, H., Wang, Y., Zhang, X.C., Wang, H., and Blarel, L. et al.: Ground-based aerosol climatology of China: Aerosol optical depths from the China Aerosol Remote Sensing Network (CARSNET) 2002–2013, Atmos. Chem. Phys., 15, 7619–7652, 2015b.

Che, H.Z., Zhao, H.J., Xia, X.A., Wu, Y.F., Zhu, J., Ma, Y.J., Wang, Y.F., Wang, H., Wang, Y.Q., Zhang, X.Y., and Shi, G.Y.: Fine Mode Aerosol Optical Properties Related to Cloud and Fog Processing over a Cluster of Cities in Northeast China, Aerosol. Air. Quality Research., 15, 2065–2081, 2015c.

Che, H.Z., Xia, X.A., Zhu, J., Wang, H., Wang, Y.Q., Sun, J.Y., Zhang, X.C., Zhang, X.Y., and Shi, G.Y.: Aerosol optical properties under the condition of heavy haze over anurban site of Beijing, China, Environ. Sci. Pollut. Res.,http://dx.doi.org/10.1007/s11356-014-3415-5, 2014.

Cheng, T., Liu, Y., Lu, D., Xu, Y., Li, H.,2006. Aerosol properties and radiative forcing in Hunshan Dake desert, northern China, Atmospheric Environment, 40, 2169-2179.

Cheng, T.T., Xu, C., Duan, J.Y., Wang, Y.F., Leng, C.P., Tao, J., Che, H.Z., He, Q.S., Wu, Y.F., Zhang, R.J., Li, X., Chen, J.M., Kong, L.D., and Yu, X.N.: Seasonal variation and difference of aerosol optical properties in columnar and surface atmospheres over Shanghai, Atmos. Environ., 123, 315-326, 2015.

Chu, D.A., Kaufman, Y.J., Ichoku, C.: Validation of MODIS aerosol optical depth retrieval over land, Geophysics Research Letters, 29 (12), 8007, 2002.

Ding, A. J., Fu, C. B., Yang, X. Q., Sun, J. N., Zheng, L. F., Xie, Y. N., Herrmann, E., Nie, W., Petäjä, T., Kerminen, V.-M., and Kulmala, M.: Ozone and fine particle in the western Yangtze River Delta: an overview of 1 yr data at the SORPES station, Atmos. Chem. Phys., 13, 5813–5830, doi:10.5194/acp-13-5813-2013, 2013a.

Ding, A. J., Fu, C. B., Yang, X. Q., Sun, J. N., Petäjä, T., Kerminen, V.-M., Wang, T., Xie, Y., Herrmann, E., Zheng, L. F., Nie, W., Liu, Q., Wei, X. L., and Kulmala, M.: Intense atmospheric pollution modifies weather: a case of mixed biomass burning with fossil fuel combustion pollution in eastern China, Atmos. Chem. Phys., 13, 10545-10554, doi:10.5194/acp-13-10545-2013, 2013b.

Ding, A. J., Huang, X., Nie, W., Sun, J. N., Kerminen, V.M., Petäjä, T., Su, H., Cheng, Y. F., Yang, X.Q., and Wang, M.H. et al.: Enhanced haze pollution by black carbon in megacities in China, Geophys. Res. Lett., 43, 2873–2879, doi: 10.1002/2016GL067745, 2016.

Duan, J., Mao, J.: Study on the distribution and variation trends of atmospheric aerosol optical depth over the Yangtze River Delta, Acta Scientiae Circumstantiae, 27 (4), 537-543, 2007.

Dubovik, O., Holben, B.N., Eck, T.F., Smirnov, A., Kaufman, Y.J., King, M.D., Tanre, D., Slutsker, I.: Variability of absorption and optical properties of key aerosol types observed in worldwide locations, J. Atmos. Sci., 59, 590–608, 2002.

Dubovik, O., King, M.D.: A flexible inversion algorithm for retrieval of aerosol optical properties from Sun and sky radiance measurements, J. Geophys. Res., 105 (D16), 20673, 2000.

Dubovik, O., Sinyuk, A., Lapyonok, T., Holben, B.N., Mishchenko, M., Yang, P., Eck, T.F., Volten, H., Munoz, O., Veihelmann, B., van der Zande, W.J., Leon, J.F., Sorokin, M., and Slutsker, I.: Application of spheroid models to account for aerosol particle nonsphericity in remote sensing of desert dust, J. Geophys. Res.-Atmos., 111 (D11), 2006.

Dubuisson, P., Buriez, J.C., and Fouquart, Y.: High spectral resolution solar radiative transfer in absorbing and scattering media, application to the satellite simulations, J. Quant. Spectrosc. Radiat.Transf., 55, 103–126, 1996.

Dubuisson, P., Roger, J.C., Mallet, M., and Dubovik, O.: A code to compute the direct solar radiative forcing: application to anthropogenic aerosols during the ESCOMPTE experiment. In: Fischer, H. (Ed.), Proceedings of the International Radiation Symposium:

Current Problems in Atmospheric Radiation. A. Deepak Publishing, Busan, Korea, 2006.

Eck, T.F., Holben, B.N., Dubovik, O., Smirnov, A., Goloub, P., Chen, H.B., Chatenet, B., Gomes, L., Zhang, X.Y., and Tsay, S.C. et al.: Columnar aerosol optical properties at AERONET sites in central eastern Asia and aerosol transport to the tropical Mid-Pacific, J. Geophys. Res., 110, 2005.

Eck, T.F., Holben, B.N., Reid, J.S., Giles, D.M., Rivas, M.A., Singh, R.P., Tripathi, S.N., Bruegge, C.J., Platnick, S., Arnold, G.T., Krotkov, N.A., Carn, S.A., Sinyuk, A., Dubovik, O., Arola, A., Schafer, J.S., Artaxo, P., Smirnov, A., Chen, H. and Goloub, P.: Fog- and Cloudinduced Aerosol Modification Observed by the Aerosol Robotic Network (AERONET), J. Geophys. Res., 117, 2012. D07206, doi: 10.1029/2011JD016839.

Eck, T. F., Holben, B. N., Sinyuk, A., Pinker, R. T., Goloub, P., Chen, H., Chatenet, B., Li, Z., Singh, R. P., and Tripathi, S. N.: Climatological aspects of the optical properties of fine/coarse mode aerosol mixtures, Journal of Geophysical Research: Atmospheres (1984–2012), 115, 19205, 2010.

Estellés, V., Campanelli, M., Utrillas, M. P., Expósito, F., and Martínezlozano, J. A.: Comparison of AERONET and SKYRAD4.2 inversion products retrieved from a Cimel CE318 sunphotometer, Atmospheric Measurement Techniques, 4, 569-579, 2012.

Fu, Q., Zhuang, G., Wang, J., Xu, C., Huang, K., Li, J., Hou, B., Lu, T., and Streets, D. G.: Mechanism of formation of the heaviest pollution episode ever recorded in the Yangtze River Delta, China, Atmospheric Environment, 42, 2023-2036, 2008.

García, O. E., Díaz, J. P., Expósito, F. J., Díaz, A. M., Dubovik, O., and Derimian, Y.: Aerosol Radiative Forcing: AERONET Based Estimates, Climate Models, edited by: Druyan, L., ISBN: 978-953-51-0135-2, InTech, 2012.

Giles, D. M., Holben, B. N., Tripathi, S. N., Eck, T. F., Newcomb, W. W., Slutsker, I., Dickerson, R. R., Thompson, A. M., Mattoo, S., and Wang, S. H.: Aerosol properties over the Indo-Gangetic Plain: A mesoscale perspective from the TIGERZ experiment, Journal of Geophysical Research Atmospheres, 116, 10--1029, 2011.

Giles, D. M., Holben, B. N., Eck, T. F., Sinyuk, A., Smirnov, A., Slutsker, I., Dickerson, R. R., Thompson, A. M., and Schafer, J. S.: An analysis of AERONET aerosol absorption properties and classifications representative of aerosol source regions, Journal of

Geophysical Research Atmospheres, 117, 127-135, 2012.

Gobbi, G. P., Kaufman, Y. J., Koren, I., and Eck, T. F.: Classification of aerosol properties derived from AERONET direct sun data, Atmospheric Chemistry & Physics, 6, 8713-8726, 2007.

Goloub, P., Li, Z., Dubovik, O., Blarel, L., Podvin, T., Jankowiak, I., Lecoq, R., Deroo, C., Chatenet, B., and Morel, J. P.: PHOTONS/AERONET sunphotometer network overview: description, activities, results, Fourteenth International Symposium on Atmospheric and Ocean Optics/Atmospheric Physics, 69360V-69360V-69315, 2007.

Gong, S.L., Zhang, X.Y., Zhao, T.L., Mckendry, I.G., Jaffe, D.A., and Lu, N.M.: Characterization of soil dust aerosol in China and its transport/distribution during 2001 ACEAsia, 2. Model simulation and validation, J. Geophys. Res., 108, 4262.http://dx.doi.org/10.1029/2002JD002633, 2003.

Gyawali, M., Arnott, W. P., Lewis, K., and Moosmüller, H.: In situ aerosol optics in Reno, NV, USA during and after the summer 2008 California wildfires and the influence of absorbing and non-absorbing organic coatings on spectral light absorption, Atmospheric Chemistry & Physics, 9, 8007-8015, 2009.

Hansen, J., Sato, M., Ruedy, R., Lacis, A., and Oinas, V.: Global warming in the twenty-first century: an alternative scenario, Proceedings of the National Academy of Sciences of the United States of America, 97, 9875-9880, 2000.

He, Q., Li, C., Geng, F., Yang, H., Li, P., Li, T., Liu, D., and Pei, Z.: Aerosol optical properties retrieved from Sun photometer measurements over Shanghai, China, Journal of Geophysical Research Atmospheres, 117, 81-81, 2012.

Holben, B. N., Eck, T. F., Slutsker, I., Tanré, D., Buis, J. P., Setzer, A., Vermote, E., Reagan, J. A., Kaufman, Y. J., Nakajima, T., Lavenu, F., Jankowiak, I., and Smirnov, A.: AERONET—A Federated Instrument Network and Data Archive for Aerosol Characterization, Remote Sensing of Environment, 66, 1-16, https://doi.org/10.1016/S0034-4257(98)00031-5, 1998.

Holben, B. N., Tanré, D., Smirnov, A., Eck, T. F., Slutsker, I., Abuhassan, N., Newcomb, W. W., Schafer, J. S., Chatenet, B., and Lavenu, F.: An emerging ground-based aerosol climatology: Aerosol optical depth from AERONET, Journal of Geophysical Research

Atmospheres, 106, 12067–12097, 2001.

Holben, B. N., Kim, J., Sano, I., Mukai, S., Eck, T. F., Giles, D. M., Schafer, J. S., Sinyuk, A., Slutsker, I., Smirnov, A., Sorokin, M., Anderson, B. E., Che, H., Choi, M., Crawford, J. E., Ferrare, R. A., Garay, M. J., Jeong, U., Kim, M., Kim, W., Knox, N., Li, Z., Lim, H. S., Liu, Y., Maring, H., Nakata, M., Pickering, K. E., Piketh, S., Redemenn, J., Reid, J. S., Salinas, S., Seo, S., Tan, F., Tripathi, S. N., Toon, O. B., and Xiao, Q.: An overview of meso-scale aerosol processes, comparison and validation studies from DRAGON networks, Atmos. Chem. Phys. Discuss., https://doi.org/10.5194/acp-2016-1182, in review, 2017.

Huang, X., Ding, A., Liu, L., Liu, Q., Ding, K., Niu, X., Nie, W., Xu, Z., Chi, X., Wang, M., Sun, J., Guo, W., and Fu, C.: Effects of aerosol–radiation interaction on precipitation during biomass-burning season in East China, Atmos. Chem. Phys., 16, 10063-10082, doi:10.5194/acp-16-10063-2016, 2016.

Hsu, N. C., Jeong, M. J., Bettenhausen, C., Sayer, A. M., Hansell, R., Seftor, C. S., Huang, J., and Tsay, S. C.: Enhanced Deep Blue aerosol retrieval algorithm: The second generation, Journal of Geophysical Research-atmospheres, 118, 9296-9315, 2013.

Ichoku, C., Chu, D. A., Mattoo, S., Kaufman, Y. J., Remer, L. A., Tanré, D., Slutsker, I., and Holben, B. N.: A spatio‐temporal approach for global validation and analysis of MODIS aerosol products, Geophysical Research Letters, 29, MOD1-1–MOD1-4, 2002.

Intergovernmental Panel on Climate Change (IPCC).Climate Change 2013. The Scientific Basis; Cambridge University Press: New York, NY, USA, 2013.

Kaufman, Y. J., Tanré, D., and Boucher, O. A.: satellite view of aerosols in the climate system, nature, 419, 215–223, 2002.

Kaufman, Y.J., Tanré, D., Remer, L.A., Vermote, E., Chu, A., and Holben, B.N.: Operational remote sensing of tropospheric aerosol over land from EOS moderate resolution imaging spectroradiometer, J. Geophys. Res., 102, 17051-17067, 1997.

Kong, S.F., Ji, Y.Q., Lu, B., Chen, L., Han, B., Li, Z.Y., and Bai, Z.P.: Characterization of PM10source profiles for fugitive dust in Fushun—a city famous for coal, Atmos. Environ., 45,5351–5365, 2011.

Lack, D. A., and Cappa, C. D.: Impact of brown and clear carbon on light absorption enhancement, single scatter albedo and absorption wavelength dependence of black carbon, Atmos. Chem. Phys., 10(9), 4207-4220, 2010.

Lee, K. H., Li, Z., Cribb, M. C., Liu, J., Wang, L., Zheng, Y., Xia, X., Chen, H., and Li, B.: Aerosol optical depth measurements in eastern China and a new calibration method, J. Geophys. Res., 115, 4038-4044, doi: 10.1029/2009JD012812, 2010.

Levy, R.C., Remer, L.A., Kleidman, R.G., Mattoo, S., Ichoku, C., Kahn, R., and Eck, T.F.: Global evaluation of the collection 5 MODIS dark-target aerosol products over land, Atmos. Chem. Phys., 10, 10399-10420, 2010.

Levy, R. C., S. Mattoo, L. A. Munchak, L. A. Remer, A. M. Sayer, F. Patadia, and Hsu, N. C.: The Collection 6 MODIS aerosol products over land and ocean, Atmos. Meas. Tech., 6(11), 2989–3034, 2013.

Li S., Wang T., Xie M., Han Y., and Zhuang B.: Observed aerosol optical depth and angstrom exponent in urban area of Nanjing, China, Atmos. Environ., 123, 350–356, 2015.

Li, W.J., Shao, L.Y., and Buseck, P.R.: Haze types in Beijing and the influence of agriculturalbiomass burning, Atmos. Chem. Phys. 10, 8119–8130, 2010.

Li, W., Li, P., Sun, G., Zhou, S., Yuan, Q. and Wang, W.: Cloud Residues and Interstitial Aerosols from Non-precipitating Clouds over an Industrial and Urban Area in Northern China, Atmos. Environ., 45, 2488–2495, doi: 10.1016/j.atmosenv.2011.02.044, 2011.

Li, W.J., Sun, J.X., Xu, L., Shi, Z.B., Riemer, N., Sun, Y.L., Fu, P.Q., Zhang, J.C., Lin, Y.T., Wang, X.F., Shao, L.Y., Chen, J.M., Zhang, X.Y., Wang, Z. F. and Wang, W.X.: A conceptual framework for mixing structures in individual aerosol particles, J. Geophys. Res., 121, 13205-13798, doi:10.1002/2016JD025252, 2016.

Li, Z., Niu, F., Lee, K., and Xin, J.: Validation and understanding of moderate resolution imaging spectroradiometer aerosol products (C5) using ground-based measurements from the handheld sun photometer network in China, J. Geophys. Res., 112,1-6, 2007.

Li, Z.Q., Eck,T., Zhang, Y., Zhang, Y.H., Li, D.H., Li, L., Xu, H., Hou, W.Z., Lv, Y., Goloub, P. and Gu, X.F.: Observations of Residual Submicron Fine Aerosol Particles Related to Cloud and Fog Processing during a Major Pollution Event in Beijing, Atmos. Environ., 86, 187–192, 2014.

Li Z., Lau, W.K.-M., Ramanathan,V., Wu,G., Ding,Y., Manoj,M.G., Liu,J., Qian,Y., Li,J., Zhou,T., Fan,J., Rosenfeld,D., Ming,Y., Wang,Y., Huang,J., Wang,B., Xu,X., Lee,S.-S., Cribb,M., Zhang,F., Yang,X.,Takemura, Wang,K., Xia,X., Yin,Y., Zhang,H.,Guo,J.,Zhai,P.M., Sugimoto,N.,Babu,S. S., and Brasseur,G.P.: Aerosol and Monsoon Climate Interactions over Asia, Rev. Geophys., doi:10.1002/2015RG000500, 2016.

Liu, Q.,Ding, W.D.,Xie, L.,Zhang, J.Q.,Zhu, J.,Xia, X.A.,Liu, D.Y.,Yuan, R.M., and Fu, Y.F.: AerosolpropertiesoveranurbansiteincentralEastChinaderivedfromgroundsun-photometer measurements, ScienceChinaEarthSciences,60, 297–314,doi: 10.1007/s11430-016-0104-3, 2017.

Lyapustin, A., Wang, Y., Xiong, X., Meister, G., Platnick, S., Levy, R., Franz, B., Korkin, S., Hilker, T., Tucker, J., Hall, F., Sellers, P., Wu, A., and Angal, A.: Scientific impact of MODIS C5 calibration degradation and C6+ improvements, Atmos. Meas. Tech., 7(12), 4353–4365, 2014.

Mishra, A.K., and Shibata, T.: Synergistic analyses of optical and microphysical propertiesof agricultural crop residue burning aerosols over the Indo-Gangetic Basin (IGB), Atmos. Environ., 57, 205–218, 2012.

Myhre, G.: Consistency between satellite-derived and modeled estimates of the direct aerosol effect, Science, 325, 187–190, 2009

Pan, L., Che, H., Geng, F., Xia, X., Wang, Y., Zhu, C., Chen,M., Gao,W., and Guo, J.: Aerosol optical properties based on ground measurements over the Chinese Yangtze Delta Region, Atmos. Environ., 44(21), 2587-2596, 2010.

Panicker, A.S., Lee, D.I., Kumkar, Y.V., Kim, D., Maki, M., Uyeda, H.: Decadal climatological trends of aerosoloptical parameters over three different environments in South Korea., Int. J. Climatol., 33, 1909–1916, 2013.

Pappalardo, G., Amodeo, A., Apituley, A., Comeron, A., Freudenthaler, V., Linné, H., Ansmann, A., Bösenberg, J., D'Amico, G., Mattis, I. Mona, L., Wandinger, U., Amiridis,V., Alados-Arboledas, L., Nicolae, D., and Wiegner, W.: EARLINET: Towards an advanced sustainable Europeanaerosol Lidar network, Atmos. Meas. Tech., 7, 2389–2409, 2014.

Remer, L.A., Kaufman, Y.J., Tanre, D., Mattoo, S., Chu, D.A., Martins, J.V., Li, R.R., Ichoku, C., Levy, R.C., Kleidman, R.G., Eck, T.F., Vermote, E., and Holben, B.N.: The MODIS aerosol algorithm, products and validation, J. Atmos. Sci., 62, 947-973, 2005.

Roger, J.-C., Mallet, M., Dubuisson, P., Cachier, H., Vermote, E., Dubovik, O., and Despiau, S.:

A synergetic approach for estimating the local direct aerosol forcing:applications to an urban zone during the ESCOMPTE experiment, J. Geophys. Res., 111, D13208, http://dx.doi.org/10.1029/2005JD006361, 2006.

Russell, P.B., Bergstrom, R.W., Shinozuka, Y., Clarke, A.D., DeCarlo, P.F., Jimenez, J.L., Livingston, J.M., Redemann, J., Dubovik, O., and Strawa, A.: Absorption Angstrom Exponent in AERONET and related data as an indicator of aerosol composition, Atmos.Chem. Phys., 10, 1155–1169, http://dx.doi.org/10.5194/acp-10-1155-2010, 2010.

Sanap, S.D., and Pandithurai, G.: Inter-annual variability of aerosols and its relationship with regional climate over Indian subcontinent, Int. J. Climatol., 35, 1041–1053, http://dx.doi.org/10.1002/joc.4037, 2014.

Schnaiter, M., Gimmler, M., Llamas, I., Linke, C., Jäger, C., and Mutschke, H.: Strong spectral dependence of light absorption by organic carbon particles formed by propanecombustion. Atmos. Chem. Phys. 6, 2981–2990, 2006.

Schwartz, S.E., and Andreae, M.O.: Uncertainty in climate change caused by aerosols, Science, 272, 1121–1122, 1996.

Shen X. J., Sun, J. Y., Zhang, X. Y., Zhang, Y. M., Zhang L., Che, H. C., Ma, Q. L., Yu, X. M., Yue, Y. and Zhang, Y. W.: Characterization of submicron aerosols and effect on visibility during a severe haze-fog episode in Yangtze River Delta, China, Atmospheric Environment, 120, 307-316, 2015.

Smirnov, A., Holben, B.N., Eck, T.F., Dubovik, O., and Slutsker, I.: Cloud screening and quality control algorithmsfor the AERONET data base, Remote Sens. Environ., 73, 337–349, 2000.

Sokolik, I. N., Toon, O. B.,1999. Incorporation of mineralogical composition into models of the radiative properties of mineral aerosol from UV to IR wavelengths, J. Geophys. Res., 104(D8), 9423-9444, doi:10.1029/ 1998JD200048.

Solomon, S., Qin, D., Manning, M., Chen, Z., Marquis, M., Averyt, K.B.,Tignor, M., Miller, and H.L.(Eds.): Climate change 2007: the physical science basis., Contribution of Working Group I to the FourthAssessment Report of the Intergovernmental Panel on Climate Change. Cambridge University Press, Cambridge, United Kingdom and New York, USA, 2007.

Soni, K., Singh, S., Bano, T., and Tanwar, R.S.: Variations in single scattering albedo and Angström absorption exponent during different seasons at Delhi, India. Atmos. Environ., 44, 4355-4363, 2010.

Takamura, T., and Nakajima, T.: Overview of SKYNET and its activities, Opt. Puray. Apl., 37, 3303–3308, 2004.

Tan, H., Wu, D., Deng, X., Bi, X., Li, F., and Deng, T.: Observation of aerosol optical depth over the Pearl River Delta, Acta Scientiae Circumstantiae., 29, 1146–1155, 2009 (in Chinese).

Tanré, D., Kaufman, Y.J., Herman, M., and Mattoo, S.: Remote sensing of aerosol properties over oceans using the MODIS/EOS spectral radiance, Journal of Geophysical Research., 102, 16971-16988, 1997.

Tao, M., Chen, L., Wang, Z., Tao, J., Che, H., Wang, X., and Wang Y.: Comparison and evaluation of the MODIS Collection 6 aerosol data in China, J. Geophys. Res. Atmos., 120, 6992–7005, doi:10.1002/2015JD023360, 2015.

Twomey, S.A., Piepgrass, M., and Wolfe, T.L.: An assessment of the impact of pollution on the global cloud Albedo, Tellus., 36B, 356-366, 1984.

Wang, L.C., Gong, W., Xia, X.A., Zhu, J., Li, J., and Zhu, Z.M.: Long-term observations of aerosol optical properties at Wuhan, an urban site in Central China, Atmos. Environ.,101, 94–102, 2015.

Wang, L.L., Xin, J., Wang, Y., Li, Z., Wang, P., Liu, G., and Wen, T.: Validation of MODIS aerosol products by CSHNET over China, Chinese Science Bulletin 52 (12), 1708-1718, 2007.

Wang, P., Che, H.Z., Zhang, X.C., Song, Q.L., Wang, Y.Q., Zhang, Z.H., Dai, X., and Yu, D.J.: Aerosol opticalproperties of regional background atmosphere in Northeast China, Atmos. Environ., 44, 4404–4412, 2010.

Wang, Z., Liu, D., Wang, Y., Wang, Z., and Shi, G.: Diurnal aerosol variations do affect daily averaged radiative forcing under heavy aerosol loading observed in Hefei, China, Atmos. Meas. Tech., 8, 2901, 2015.

Wehrli, C.: Calibration of filter radiometers for the GAW Aerosol Optical Depth network at Jungfraujoch and Mauna Loa. In: Proceedings of ARJ Workshop,SANW Congress, Davos, Switzerland, pp. 70-71,2002.

Wu, L.X.,Lü, X., Qin, K., Bai, Y., Li, J.L., Ren, C.B., and Zhang, Y.Y.: Analysis to Xuzhou aerosol optical characteristics with ground-based measurements by sun photometer (in Chinese), Chin Sci Bull, 61: 2287–2298, doi: 10.1360/N972015-00874, 2016.

Xia, X., Chen, H., Goloub, P., Zong, X., Zhang, W., and Wang, P.: Climatological aspects of aerosol opticalproperties in North China Plain based on ground and satellite remote-sensing data, J. Quant. Spectrosc.Radiat.Transf., 127, 12–23, 2013.

Xia, X., Li, Z., Holben, B., Wang, P., Eck, T., Chen, H., Cribb, M., and Zhao, Y.: Aerosol optical properties and radiative effects in the Yangtze Delta region of China, J. Geophys. Res., 112, D22S12, doi:10.1029/2007JD008859, 2007.

Xiao, Q., Zhang, H., Choi, M., Li, S., Kondragunta, S., Kim, J., Holben, B., Levy, R. C., and Liu, Y.: Evaluation of VIIRS, GOCI, and MODIS Collection 6 AOD retrievals against ground sunphotometer observations over East Asia, Atmos. Chem. Phys., 16, 1255-1269, doi:10.5194/acp-16-1255-2016, 2016.

Xie, Y., Zhang, Y., Xiong, X.X, Qu, J.J., and Che, H.Z.: Validation of MODIS aerosol optical depth product over China using CARSNET measurements, Atmos. Environ., 45, 5970-5978, 2011.

Xin, J., Wang, Y., Li, Z., Wang, P., Hao, W., Nordgren, B., Wang, S., Liu, G., Wang, L., Wen, T., Sun, Y., and Hu, B.: Aerosoloptical depth (AOD) and angstrom exponent of aerosols observed by the Chinese Sun Hazemeter Networkfrom August 2004 to September 2005, J. Geophys. Res., 112 (D05203), 2007.

Xin, J.Y., Zhang, Q., Gong, C.S., Wang, Y.S., Du, W.P., and Zhao, Y.F.: Aerosol direct radiative forcing over Shandong Peninsula in East Asia from 2004 to 2011, Atmos. Ocean. Sci. Lett., 7, 74-79, 2014.

Yan, P., Pan, X.L., Tang, J., Zhou, X.J., Zhang, R.J., and Zeng, L.M.: Hygroscopic growth ofaerosol scattering coefficient: a comparative analysis between urban and suburbansites at winter in Beijing, Particuology, 7, 52–60,2009.

Yang, M., Howell, S.G., Zhuang, J., and Huebert, B.J.: Attribution of aerosol light absorption to black carbon, brown carbon, and dust in China – interpretations of atmospheric measurements during EAST-AIRE, Atmos. Chem. Phys., 9, 2035–2050, http://www.atmos-chem-phys.net/9/2035/2009/, doi:10.5194/acp-9-2035-2009, 2009.

Zhang, L., Sun, J. Y., Shen, X. J., Zhang, Y. M., Che, H., Ma, Q. L., Zhang, Y. W., Zhang, X. Y., and Ogren, J. A.: Observations of relative humidity effects on aerosol light scattering in the Yangtze River Delta of China, Atmos. Chem. Phys., 15, 8439-8454, doi:10.5194/acp-15-8439-2015, 2015.

Zhang, Q., Streets, D., Carmichael, G., He, K., Huo, H., Kannari, A., Klimont, Z., Park, I.S., Reddy, S., Fu, J., Chen, D., Duan, L., Lei, Y., Wang, L., and Yao, Z.L.: Asian emissions in 2006 for the NASA INTEX-B mission, Atmos. Chem. Phys., 9,5131-5153, doi:10.5194/acp-9-5131-2009, 2009.

Zhang, X., Wang, Y., Niu, T., Zhang, X., Gong, S., Zhang, Y., and Sun, J.: Atmospheric aerosol compositions in China: spatial/temporal variability, chemical signature, regional haze distribution and comparisons with global aerosols. Atmos. Chem. Phys., 12, 779–799, http://dx.doi.org/10.5194/acp-12-779-2012, 2012.

Zhao, H., Che, H., Ma, Y., Xia, X., Wang, Y., Wang, P, and Wu, X.: Temporal variability of the visibility, particulate matter mass concentration and aerosol optical properties over an urban site in Northeast China. Atmos. Res., 166, 204-212, 2015.

Zhao, H., Che, H., Zhang, X., Ma, Y., Wang, Y., Wang, X., Liu, C., Hou, B., and Che, H.: Aerosol optical properties over urban and industrial region of Northeast China by using ground-based sun-photometer measurement. Atmos. Environ., 75, 270–278, 2013.

Zhu, J., Che, H., Xia, X., Chen, H.B, Goloub, P., and Zhang, W.: Column-integrated aerosol optical and physical properties at a regional background atmosphere in North China Plain. Atmos. Environ., 84,54–64, 2014.

Zhuang, B., Wang, T., Li, S., Liu, J., Talbot, R., Mao, H., Yang, X., Fu, C., Yin, C., Zhu, J., Che, H., and Zhang, X.: Optical properties and radiative forcing of urban aerosols in Nanjing over China. Atmos. Environ., 83, 43–52, 2014.